Journal of Applied Pharmaceutical Science Vol. 13(02), pp 124-145, February, 2023
Available online at http://www.japsonline.com
DOI: 10.7324/JAPS.2023.130215
ISSN 2231-3354

Ailanthus excelsa leaf extract: Chemical characterization, antischistosomal activity, and *in silico* study of isolated phenolic compounds as promising thioredoxin glutathione reductase inhibitors

Hala Sh. Mohammed[1], Samia William[2], Tarek Aboushousha[3], Hoda M. Abu Taleb[4], Rehab Sabour[5], Mosad A. Ghareeb[6*]

[1]Department of Pharmacognosy and Medicinal Plants, Faculty of Pharmacy (Girls), Al-Azhar University, Cairo, Egypt.
[2]Department of Parasitology, Theodor Bilharz Research Institute, Giza, Egypt.
[3]Department of Pathology, Theodor Bilharz Research Institute, Giza, Egypt.
[4]Department of Environmental Research, Theodor Bilharz Research Institute, Giza, Egypt.
[5]Department of Medicinal Pharmaceutical Chemistry and Drug Design, Faculty of Pharmacy (Girls), Al-Azhar University, Cairo, Egypt.
[6]Department of Medicinal Chemistry, Theodor Bilharz Research Institute, Egypt.

ARTICLE INFO

Received on: 23/07/2022
Accepted on: 16/10/2022
Available Online: 05/02/2023

Key words:
Ailanthus excelsa, polyphenolics, LC-ESI-MS/MS, antischistosomal activity, TGR, docking.

ABSTRACT

Hepatic schistosomiasis is the most well-known chronic condition, with a variety of clinical symptoms. In the current study, the metabolite profile of the *Ailanthus excelsa* leaf butanol extract was investigated using chromatographic isolation and Liquid chromatography electrospray ionization /mass spectrometry (LC-ESI-MS/MS) analysis. Also, its schistosomicidal effect was examined *in vivo* regarding disease progression in a comparative experimental study to praziquantel (PZQ). The parasitological parameters (total worm burden, tissue egg load, and oogram pattern) of the infected and the treated mice were counted. A histopathological examination of the liver granuloma took place as well. The extract (at a dose of 500 mg/kg) caused a significant worm reduction of 41.30% and also a significant reduction in intestinal egg load (6.36 ± 1.12 *vs.* 17.82 ± 2,024.6). Data also showed a reduction in immature eggs in the extract group (33.00 ± 2.45 *vs.* 57.4 ± 3.89) when compared to the infected untreated group. Five phenolic compounds were isolated and identified as gallic acid (1), methyl gallate (2), quercitrin (3), isoquercitrin (4), and kaempferin (5). Furthermore, molecular docking was utilized for the first time to evaluate the efficacy of the isolated compounds (1–5) in disrupting the essential worm enzyme thioredoxin glutathione reductase. Compounds 3–5 showed high docking scores ranging from −7.054 to −11.370 kcal/mol that were comparable to that of PZQ (−6.407 kcal/mol). Moreover, LC-ESI-MS/MS profiling led to the identification of 33 secondary metabolites. These compounds were classified as phenolic acids, flavonoids, iridoids, stilbenoids, chalcones, tannins, and coumarins. The findings suggest that the *A. excelsa* leaf extract could be used as a naturally occurring antischistosomal agent and this emphasizes the significance of phenolic components.

INTRODUCTION

Schistosomiasis is endemic in 75 countries in Africa, Asia, South America, and the Middle East, rendering it one of the most important neglected tropical illnesses (Gray *et al*., 2011; Hotez and Kamath, 2009). In the control of schistosomiasis, the use of safe and effective drugs will remain the main control tool until a successful vaccine is produced. Praziquantel (PZQ) is one

*Corresponding Author
Mosad A. Ghareeb, Medicinal Chemistry Department, Theodor Bilharz Research Institute, Giza, Egypt.
E-mail: m.ghareeb @ tbri.gov.eg

of the most important and widely effective antibilharzial drugs against humans' four main pathogenic schistosomes (Gönnert and Andrews, 1977), and it has proven effective in large-scale therapies. Population-level schistosomiasis control with PZQ has various drawbacks. PZQ susceptibility has been recently implemented in schistosomes by laboratory selection (Fallon and Doenhoff, 1994). Reduced cure rates and failure of treatment after PZQ were reported in Senegalese, Kenyan, and Egyptian patients (Ismail *et al*., 1994). However, *Schistosoma* developed resistance to PZQ; in endemic regions, PZQ-resistant parasites had been established. Therefore, it is essential to develop new therapeutics for the treatment of schistosomiasis (Doenhoff *et al*., 2008). Natural products have risen to power in recent years as potential sources of novel schistosomiasis medications (El-Sayed *et al*., 2011). This article attempts to update the antischistosomal natural products and/or derived compounds. *Ailanthus excelsa* (*A. excelsa*) (Roxb.) belongs to the Simaroubaceae family and is a deciduous tree commonly known as the "tree of heaven." The plant is widely distributed throughout Asia and North Australia, and it is indigenous to China (Adamik and Brauns, 1957; Khushbu *et al*., 2011). Traditionally, various parts of *A. excelsa* are used to treat a variety of health problems, such as wounds and skin eruptions, fevers, bronchitis, asthma, diarrhea, and dysentery (Asolkar *et al*., 1992; British Pharmacopoeia, 1988). *Ailanthus excelsa* has also been used as a source of medication. For example, in Chinese medicine, the bark is used to treat diarrhea and dysentery, particularly when there is blood in the stool (Dash and Padhy, 2006). In Asian and Australian medicine, the bark has also been used for worms, excess vaginal discharge, malaria, and asthma (Chevellier, 1996; Kirtikar and Basu, 1995). In Africa (Sharma and Guna-Vijnana, 1996), the plant is useful in the treatment of gonorrhea, epilepsy, tapeworm infection, and high blood pressure (Sharma and Guna-Vijnana, 1996). *Ailanthus excelsa* contains a wide range of phytochemicals, including quassinoids, alkaloids, flavonoids, terpenoids, and proteins (Joshi *et al*., 2003; Kapoor *et al*., 1971; Loizzo *et al*., 2007; Nag and Matai, 1994; Ogura *et al*., 1977; Said *et al*., 2010; Sherman *et al*., 1980). Moreover, β-sitosterol and vitexin were isolated from the leaf part (Kapoor *et al*., 1971). From a biological activity point of view, the plant possesses a wide spectrum of biological activities, such as analgesic (Khushbu *et al*., 2011), antimicrobial (Ghumare *et al*., 2014; Manikandan *et al*., 2015), antidepressant (Chauhan *et al*., 2011), anticancer (Ogura *et al*., 1977; Said *et al*., 2012), antifungal (Joshi *et al*., 2003; Ratha *et al*., 2013), antidermatophytic (Pandith, 2012), antiviral (Rashed *et al*., 2013), antioxidant (Said *et al*., 2010), antiproliferative (Said *et al*., 2010), hepatoprotective (Hukkeri *et al*., 2002), antiasthmatic (Kumar *et al*., 2010), antidiabetic (Cabrera *et al*., 2008), and antibacterial (Shrimali *et al*., 2001). The root bark has also been shown to have significant cytotoxic and anticancer properties (Ogura *et al*., 1977). For schistosome survival inside the mammalian host, the parasite selenoprotein thioredoxin glutathione reductase (TGR) is required. Several inhibitors of *Schistosoma mansoni* TGR have been discovered through high-throughput screening programs (Alger and Williams, 2002). A flavoprotein is homodimeric where a glutaredoxin (Grx) domain is linked to a normal thioredoxin reductase (TR) domain in each subunit. In *Schistosoma*, the schistosomal redox homeostasis is dependent entirely on TGR, which guides nicotinamide adenine dinucleotide phosphate to reduce equivalents to thioredoxin and glutathione (Alger and Williams, 2002). TGR is the only enzyme that can reduce both thioredoxin and glutathione disulfide, implying that the parasite's redox mechanism is heavily reliant on it. Due to the relevance of biological redox systems and the variations in redox metabolism between *S. mansoni* and its host (Kuntz *et al*., 2007), TGR could be an essential parasite protein and therapeutic target. The polyphenolic components of the *n*-butanol extract of *A. excelsa* leaves were characterized and their antischistosomal activity *in vivo* was investigated in the current study. Additionally, isolated chemicals were molecularly docked as strong TGR inhibitors.

MATERIALS AND METHODS

Plant materials

In May 2019, leaves of *A. excelsa* (Roxb.) were collected from the Zoo Garden in Giza Governorate, Egypt. Dr. Therese Labib, Consultant at Orman Botanical Garden in Giza, Egypt, and the National Gene Bank, graciously recognized the plant. The Herbarium of the Medicinal Chemistry Department, Theodor Bilharz Research Institute, Giza, Egypt, received a voucher specimen (No. A.e/L/2019).

Extraction, fractionation, and chromatographic isolation

Dry powdered leaves of *A. excelsa* (2 kg) were extracted with ethanol at room temperature. A rotavapor was used to concentrate the crude extract under reduced pressure to afford 420 g (a yield of 21%). The ethanolic extract was defatted using petroleum ether (60°C–80°C) (400 g). The residue (375 g) was dissolved in distilled water and then consecutively extracted with CH_2Cl_2, ethyl acetate, and *n*-butanol to afford 65, 38, 74, and 105 g, respectively, for CH_2Cl_2, ethyl acetate, *n*-butanol, and aqueous extracts (Mohammed *et al*., 2019). The *n*-butanol extract (55 g) was subjected to polyamide column chromatography and eluted with H_2O/ethanol via a gradient mix elution system with gradually decreasing polarity up to 100% ethanol. One hundred ninety-eight individual fractions were obtained and were combined according to their chemical profiles on paper chromatography (PC) and/or thin-layer chromatography. The main fractions were further purified by successive Sephadex LH-20 column chromatography using different mobile phases: BIW (4:1:5 v/v/v upper layer), 20% ethanol, and 100% ethanol to afford five pure, isolated compounds.

In vivo anti-schistosomal study

Animals

Forty laboratory male Swiss albino mice (CD-1) aged 6–7 weeks with a weight range of 18–20 g were obtained from the Schistosome Biological Supply Centre (SBSC), Theodor Bilharz Research Institute, Giza, Egypt. They were then housed in an appropriate environment at 20°C–22°C with a 12 hours light/dark cycle and a humidity range of 50%–60%. During acclimatization and experimental periods, mice were provided with food and water *ad libitum*.

Infection of animals

The cercarial suspension (0.1 ml) was gently mixed, stained with a picric acid solution, and counted. Infection of mice with *S. mansoni* cercariae was conducted using the body immersion method and through exposure to 60–10 cercariae/mouse (Liang *et al*., 1987).

Compounds assessed *in vivo*

The *A. excelsa* leaf extract and PZQ were evaluated for their antischistosomal activity *in vivo*. PZQ was obtained as tablets (Distocide, Egyptian International Company, EIPICO, Egypt). Both were freshly suspended in 2% Cremophor EL before use.

Experimental design

The *A. excelsa* leaf extract and PZQ were orally administered for five consecutive days in the seventh week after infection.

Group 1: *S. mansoni*-infected mice (infected control).
Group 2: Infected mice were administered PZQ at a dose of 200 mg/kg.
Group 3: Infected mice were administered *A. excelsa* extract at a dose of 200 mg/kg.
Group 4: Infected mice were administered *A. excelsa* extract at a dose of 500 mg/kg.

Antischistosomal activity

Mice were sacrificed and tamed; after that, the worm burden was estimated and sexed to estimate worm reduction proportion (Duvall and De Witt, 1967). Liver or intestinal tissues were examined to count the number of eggs per gram (Kamel et al., 1977). During various stages, the percentage of egg production was calculated, and then three parts of the intestine were studied to identify and count the eggs in various stages of maturation, accompanied by calculating the average numbers for each stage (Pellegrino *et al*., 1962).

Histopathological investigations

Histopathological investigations were performed according to the reported procedures with some modifications (Ibrahim *et al*., 2022).

Molecular docking study

The Molecular Operating Environment (MOE-DOCK/2014.09) was used for molecular modeling. All compounds were sketched using the ChemDraw program and subjected to an energy minimization process to be introduced into MOE, where the conformational search was performed. Their 3D conformers were then docked into the active site of the TGR enzyme [protein data bank (PDB) ID: 2V6O]. During the docking process, London dG was kept for ranking, and Generalized Born Volume Integral/ Weighted Surface Area dG was utilized for scoring the generated poses. Water molecules were deleted. With default parameters, the docking process was used. London dG ranked the top 30 poses, and they were stored.

Statistical analysis

All data were entered and analyzed in the Statistical Package for the Social Sciences (SPSS) software (IBM SPSS Statistics for Windows, Version 23, IBM Corp., Armonk, NY).

RESULTS AND DISCUSSION

Chromatographic isolation and chemical profiling of the *n*-butanol extract using Liquid chromatography electrospray ionization /mass spectrometry (LC-ESI-MS/MS) analysis

Five phenolic metabolites were isolated from *n*-butanol as a polyphenolic-rich extract using successive column chromatography. Spectroscopic approaches such as ^{1}H- and carbon-13 magnetic resonance (^{13}C-NMR), as well as chemical tests, were utilized to determine their chemical structures (Fig. 1, 4S–11S). The chemical metabolites were tentatively identified using LC-ESI-MS/MS analysis in the negative ion mode based on their MS fragmentation patterns, molecular weights, and previous data (Table 1 and Fig. 1S, 12S–15S). The examined extract included 33 secondary metabolites in total; the identified secondary metabolites were classified as phenolic acids, organic acids, flavonoids (aglycones and glycosides), iridoids, stilbenes, chalcones, tannins, and coumarins (Supplementary Materials: 2S).

Characterization of the isolated compounds

3,4,5-trihydroxy benzoic acid (gallic acid)

Off-white amorphous powder, m.p.: 250ºC–253ºC. The proton magnetic resonance (^{1}H-NMR) spectrum [400 megahertz (MHz), dimethyl sulfoxide (DMSO)-d_6] showed aromatic proton resonance at δ_H ppm; 6.93 (2H, s, H-2/6) as well as a hydroxyl

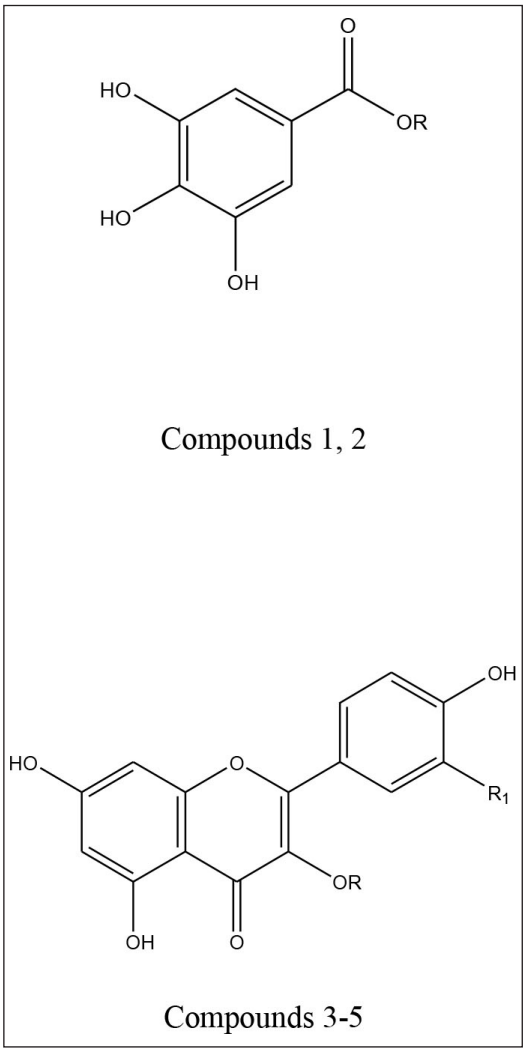

Figure 1. Chemical structures of phenolic compounds isolated from the *A*. excelsa leaf extract. Gallic acid (1); *R* = H. Methyl gallate (2); *R* = CH3. Quercitrin (3); *R* = α-L-rhamnopyranosyl, R1 = OH. Isoquercitrin (4); *R* = β-D-glucopyranosyl, R1 = OH. Kaempferin (5); *R* = α-L-rhamnopyranosyl, R1 = H.

Table 1. Tentative identification of secondary metabolites in the *A. excelsa* leaf extract using LC-ESI-MS/MS in the negative ion mode.

Peak No.	Rt	*m/z* [M-H]$^-$	M.wt.	M.F.	Ms^n fragments	Tentatively identified compounds	References
1	0.77	133	134	$C_4H_6O_5$	115	Malic acid	Ghareeb *et al.* (2018a)
2	0.82	191	192	$C_7H_{12}O_6$	173, 127, 111	Quinic acid	Ghareeb *et al.* (2018a); Sobeh *et al.* (2018)
3	0.98	169	170	C7H6O5	125, 97	Gallic acid	Ghareeb *et al.* (2019)
4	1.17	169	170	$C_7H_6O_5$	125, 97	Gallic acid	Ghareeb *et al.* (2019)
5	2.09	153	154	$C_7H_6O_4$	109, 97, 81	Protocatechuic acid	Ghareeb *et al.* (2018a)
6	3.73	137	138	$C_7H_6O_3$	93	Salicylic acid	Ghareeb *et al.* (2018a)
7	4.28	183	184	$C_8H_8O_5$	169, 125	Methyl gallate	Ghareeb *et al.* (2018b)
8	5.99	367	368	$C_{17}H_{20}O_9$	193, 191, 173	4-*O*-Feruloylquinic acid	Bakchiche *et al.* (2019)
9	6.17	337	338	$C_{16}H_{18}O_8$	191	*p*-Coumaroylquinic acid	Nandutu *et al.* (2007)
10	6.53	361	362	$C_{19}H_{22}O_7$	321, 315, 291, 259	Ligstroside	Tasioula-Margari and Tsabolatidou, (2015)
11	6.82	167	168	$C_8H_8O_4$	152, 123, 107, 95	Vanillic acid	Kumar *et al.* (2017)
12	7.36	447	448	$C_{21}H_{20}O_{11}$	301, 255, 179	Quercetin-3-*O*-rhamnoside	Li *et al.* (2018)
13	7.91	463	464	$C_{21}H_{20}O_{12}$	301, 271, 179	Quercetin 3-*O*-glucoside	Ghareeb *et al.* (2018a)
14	7.98	431	432	$C_{21}H_{20}O_{10}$	285, 179, 151	Kaempferol-3-*O*-rhamnoside	Barros *et al.* (2011)
15	8.30	209	210	$C_{10}H_{10}O_5$	191	5-Hydroxyferulic acid	Ghareeb *et al.* (2018a)
16	8.43	193	194	$C_{10}H_{10}O_4$	178, 149, 134, 116	Ferulic acid	Goufo *et al.* (2020)
17	8.99	243	244	$C_{14}H_{12}O_4$	225, 215, 201, 199, 181, 175, 159	*trans*-Piceatannol	Goufo *et al.* (2020)
18	9.44	285	286	$C_{12}H_{13}O_8$	153, 152, 108, 109	Protocatechuic acid-*O*-arabinoside	Ammar *et al.* (2015)
19	9.83	177	178	$C_{10}H_9O_3$	145, 118	*p*-Coumaric acid methyl ester	Šuković *et al.* (2020)
20	11.22	327	328	$C_{18}H_{16}O_6$	312, 297	5-Hydroxy-3',4',7-trimethoxyflavone	Simirgiotis *et al.* (2015)
21	11.99	327	328	$C_{18}H_{16}O_6$	312, 297	5-Hydroxy-3′,4′,7-trimethoxyflavanone	Simirgiotis *et al.* (2015)
22	14.10	311	312	$C_{13}H_{12}O_9$	179, 148	Caftaric acid	Ghareeb *et al.* (2018c)
23	17.63	181	182	$C_9H_{10}O_4$	137	Dihydrocaffeic acid	Magana *et al.* (2020)
24	19.31	311	312	$C_{15}H_{20}O7$	179, 135	Caffeic acid pentoside	Reed *et al.* (2009)
25	19.49	311	312	$C_{15}H_{20}O_7$	179, 135	Caffeic acid pentoside	Reed *et al.* (2009)
26	19.56	161	162	$C_9H_6O_3$	121	4-Hydroxycoumarin	Chanda et al. (2020)
27	19.68	311	312	$C_{20}H_{40}O_2$	267	Arachidic acid	Simirgiotis *et al.* (2015)
28	20.07	353	354	$C_{16}H_{18}O_9$	191, 179, 173, 161, 135	Chlorogenic acid	Ma *et al.* (2020)
29	21.06	325	326	$C_{15}H_{18}O_8$	163, 119	*p*-Coumaroyl hexose (*cis*-melilotoside)	Olennikov *et al.* (2018)
30	24.85	271	272	$C_{16}H_{14}O_4$	137, 106	*p*-Hydroxyphenethyl anisate	Ma *et al.* (2020)
31	29.15	327	328	$C_{19}H_{20}O_5$	228, 212	Selinidin	Ma *et al.* (2020)
32	29.33	255	256	$C_{15}H_{12}O_4$	135,119	Isoliquiritigenin/liquiritigenin	Wang *et al.* (2020)
33	30.23	477	478	$C_{22}H_{22}O_{12}$	441, 313, 289, 269, 169, 151	2-*O*-*p*-Coumaroyl-1-*O*-galloy-β-D-glucose	Wang *et al.* (2020)

proton of the carboxylic acid group at 12.30. The ^{13}C-NMR spectrum (100 MHz, DMSO-d6) showed carbon resonances at δC ppm; 120.90 (C-1, quaternary aromatic carbon), 109.20 (C-2 and 6, two symmetric aromatic methine carbons), 146.13 (C-3 and 5, two symmetric oxygenated aromatic carbons), 139.02 (C-4, oxygenated carbon), and 166.82 (C-7, carbonyl group). As a result, metabolite 1 was identified as gallic acid (Eldahshan, 2011).

Methyl 3,4,5-trihydroxy benzoate (methyl gallate)

White fine crystals, m.p.: 198ºC–201ºC. It showed a dark violet spot-on PC under long UV light. The ^{1} H-NMR spectrum (400 MHz, DMSO-d6) demonstrated a typical signal of two symmetrical aromatic protons at δ_H ppm; 6.94 (2H, s, H-2/6) and the aliphatic methoxy protons at 3.53 (3H, s, -OCH3). The ^{13}C-NMR spectrum (100 MHz, DMSO-d6) showed carbon resonances at δC ppm; 49.60 (-OCH_3) and aromatic carbon signals at 109.0 (C-2 and 6), 121.0 (C-1), 138.50 (C-4), and 146.63 (C-3 and 5) and carbonyl carbon was detected at δ_C 167.71 (-CO). Thus, metabolite 2 was identified as methyl gallate (Choi *et al*., 2014).

Quercetin3-O-α-L-rhamnopyranoside (Quercitrin)

Yellow amorphous powder. It showed a dark purple spot (long/short UV) that changed to yellow fluorescence (UV/NH_3). The ^{1}H-NMR spectrum (400 MHz, DMSO-d_6): δ_H ppm 12.7 (1H, s, OH-5), 7.31 (1H, brs, H-2′), 7.25 (1H, brd, hidden by H-2′ signal, H-6′), 6.87 (1H, d, J = 8.4 Hz, H-5’), 6.37 (1H, d, *J* = 1.8 Hz, H-8), 6.22 (1H, d, *J* = 2.1 Hz, H-6), 5.26 (1H, brs, H-1″), 3.80-3.12 (the remaining sugar protons), and 0.82 (3H, d, *J* = 6 Hz, Me-6″). From the above data, metabolite 3 exhibited two spin coupling systems characteristic of quercetin, a glycone. The first one was ABX for tree types of protons H-2′,6′ and 5′ of a 3′,4′-dihydroxy B-ring. The second one was a 2 brs signal of two *meta*-coupled protons H-6 and 8 in a 5,7-dihydroxy A-ring (Mabry *et al*., 1970). In the aliphatic region, δ_H at 5.26 (1H, brs, H-1″) assigned for 3-*O*-α-configuration and at 0.82 (d, *J* = 6 Hz, 6″-CH_3) were indicative of the *O*-α-*L*-rhamnopyranosyl moiety. Therefore, metabolite 3 could be defined as quercetin 3-*O*-*L*-rhamnopyranoside (quercitrin).

Quercetin 3-O-β-D-glucopyranoside (Isoquercitrin)

Yellow amorphous powder. It displayed a dark purple spot (long/short UV) that changed to yellow fluorescence (UV/NH_3). The ^{1}H-NMR spectrum (400 MHz, DMSO-d_6): δ_H ppm 12.69 (1H, s, OH-5), 7.64 (1H, brs, H-2′), 7.62 (1H, brd, hidden by H-2′ signal, H-6′), 6.88 (1H,d, *J* = 8.4 Hz, H-5′), 6.45 (1H, brs, H-8), 6.22 (1H, d, brs, H-6), 5.33 (1H, d, *J* = 7 Hz, H-1″), and 3.65–3.14 (the remaining sugar protons). The ^{13}C-NMR spectrum (100 MHz, DMSO-d_6): δ_C ppm 177.90 (C-4), 164.60 (C-7), 161.70 (C-5), 156.63 (C-2), 156.78 (C-9), 148.92 (C-4′), 145.27 (C-3′), 133.77 (C-3), 122.06 (C-6′), 121.62 (C-1′), 116.66 (C-5′), 115.66 (C-2), 104.43 (C-10), 101.31 (C-1″), 99.12 (C-6), 93.96 (C-8), 78.03 (C-5″), 76.96 (C-3″), 74.55 (C-2″), 70.39 (C-4″), and 61.43 (C-6″). According to these findings, metabolite 4, like metabolite 3, contained two spin coupling systems in an aromatic region (Mabry *et al*., 1970). The aliphatic region showed an anomeric proton at δ_H 5.39 (1H, d, J = 7 Hz, H-1′’) assigned for 3-*O*-β-glucopyranoside and confirmed by six carbon resonances in the ^{13}C-NMR spectrum agreeing with the previously reported data. In addition, 15 carbon resonances typical of the quercetin moiety were assigned in the aromatic region, among which the two key signals of quercetin, a glycone, were assigned at 148.92 (C-4′) and 145.27 (C-3′) ppm (Agrawal, 1989; Harborne and Mabry, 1982). The characteristic position of C-3 at 133.77 ppm confirms the *O*-glucosidation at C-3. Accordingly, metabolite 4 was identified as quercetin 3-*O*-β-glucopyranose (isoquercitrin).

Kaempferol 3-O-α-L-rhamnopyranoside (Kaempferin)

Yellow amorphous powder. It displayed a dark purple spot (long/short UV) that turned to yellow fluorescence (UV/NH_3). The ^{1}H-NMR spectrum (400 MHz, DMSO-d_6): δ_H ppm 8.07 (2H, d, J = 8.5 Hz, H-2′/ 6′), 6.92 (2H, d, J = 8.5 Hz, H-3′/ 5′), 6.60 (1H, d, *J* = 1.7 Hz, H-8), 6.40 (1H, d, *J* = 1.7 Hz, H-6), 5.37 (1H, brd, H-1″), 3.85-3.17 (the rest of the signals of the rhamnosyl protons), and 1.13 (3H, d, *J* = 6.8 Hz H-6″). The ^{13}C-NMR spectrum (100 MHz, DMSO-d_6): δ_C ppm 176.03 (C-4), 161.32 (C-7), 160.32 (C-5), 159.30 (C-4′), 155.85 (C-2,9), 137.37 (C-3), 136.05 (C-2′/6′), 121.47 (C-1′), 115.40 (C-3′/5′), 104.62 (C-10), 100.7 (C-1″), 98.74 (C-6), 94.25 (C-8), 71.58 (C-4″), 70.23 (C-2″), 69.99 (C-3″), 69.79 (C-5″), and 17.85 (C-6″). Based on the chromatographic characteristics, metabolite 5 was predicted to be a kaempferol–glycoside, as indicated by the shift in fluorescence to dull yellow upon fuming with ammonia vapor. The ^{1}H-NMR spectrum revealed an A_2X_2 spin coupling system of two ortho doublets; two protons each were assigned at δH 8.07 and 6.92 with *J*-values of 8.5 Hz for H-2′/6′ and H-3′/5′, respectively, of a 1,4-disubstituted B-ring. Also, two meta doublets, one proton each, were established for H-8 and H-6 at 6.60 and 6.40 (*J* = 1.7 Hz), respectively, of a 5,7-dihydroxy A-ring. In the aliphatic region, an anomeric proton 5.37 (1H, brd, H-1″), also a doublet methyl proton, with a *J*-value of 6.8 Hz was assigned for CH_3-6″ of the rhamnose moiety. The ^{13}C-NMR spectrum showed 13 carbon resonances characteristic of kaempferol aglycone (Agrawal, 1989; Harborne and Mabry, 1982), among which were five key signals at δC 176.03 (C-4) and 137.37 (glycosylated C-3) of the C-ring and 159.30 (hydroxylated C-4′), 136.05 (C-2′/6′), and 115.40 (C-3′/5′) of the B-ring. In addition, anomeric carbon resonance at δC 100.7 was assigned for C-1″; the remaining carbon resonances in the aliphatic region at δ_C 71.58 (C-4″), 70.23 (C-2″), 69.99 (C-3″), 69.79 (C-5″), and 17.85 (C-6″) were assigned for the –*O*-α-*L*-rhamnopyranosyl moiety at C-3 from its downfield shift (Δ≈+1.5 ppm) (Agrawal, 1989; Harborne and Mabry, 1982). Therefore, metabolite 5 was identified as kaempferol-3-*O*-α-*L*-rhamnopyranoside (kaempferin).

***In vivo* anti-schistosomal activity**

Worm burden and distribution

Administering PZQ at an oral dose of 200 mg/kg to *S. mansoni*-infected mice for five consecutive days was effective in reducing total worm counts (93.5% worm reduction), while *A. excelsa* extract administration at doses of 200 and 500 mg/kg reduced total worm counts (33.2% and 41.3% worm reduction, respectively). The difference was statistically significant at $p < 0.01$ (Table 2).

Tissue egg load

In comparison to PQZ (200 mg/kg body weight), mice given *A. excelsa* at doses of 200–500 mg/kg body weight showed

a greater reduction in mean total tissue (hepatic and intestinal). The difference between the infected and untreated control mice (10,938.41911.32 and 17,815.002024.66) was statistically significant at $p < 0.01$ (Table 3).

Percentage of egg developmental stages (oogram pattern)

PZQ at 200 mg/kg was given to *S. mansoni*-infected mice for five consecutive days, and this revealed the disappearance of all immature stages of ovary development with an increase in the dead ova. The difference was significant between the infected and untreated mice at $p < 0.01$ (Table 3). Regarding the total immature eggs, a significant decrease in the percentage was observed upon using the *A. excelsa* extract, and an increase in the percentage of dead and mature eggs was observed when compared with the infected group.

Hepatic granuloma volume

Histopathological investigation of liver segments from various examined groups showed a meaningful reduction in the number of egg granulomas in the PZQ-treated group in relation to all other treated and control groups ($p < 0.01$). However, no significant difference in granuloma counts was found between the control and treated groups at either of the doses assessed (200 and 500). As regards the granuloma diameter, there was a significant reduction in granuloma size in the PZQ- and *A. excelsa*-treated groups (500 mg/kg) compared to the control group (4,222.366.52 m). There was no statistically significant difference in granuloma diameter between the control and *A. excelsa*-treated groups (200 mg/kg). In addition, most of the egg granulomas of diverse groups were fibrocellular, with a mild increase in the number of cellular granulomas in the control group compared to the other treated groups. Worm granulomas could be detected only in the PZQ-treated group. Considering the measurement of liver fibrosis in tissue sections, it was found that the PZQ-treated group showed a significant reduction in fibrosis [measured as area/ low-power field (LPF)] compared to the control group. The *A. excelsa*-treated group (500) showed a less significant reduction in fibrosis than the control group relative to the PZQ-treated group. No considerable variation in fibrosis was noticed between the control and the *A. excelsa*-treated group (200). Studying the cellular pattern of inflammatory cells showed a predominance of neutrophils over mononuclear inflammatory cells (Table 4 and Figures 2 and 3). Herbal medicines are of immense importance as a vital source of bioactive compounds, which are the basic nucleus of the pharmaceutical industry (Phillipson, 1994). Moreover, the efficacy of antischistosomiasis drugs is inferred by the reduced egg and worm burden index in the treated mice (Andrews, 1985). Consequently, the reduction rate of eggs in the mice treated with PZQ is a strong indicator of the drug's efficacy. Furthermore, our study of the *A. excelsa* extract recorded a reduction in egg count after treatment. The reduced egg load in the treated mice may be due to several factors, including reduced worm burden, decreased productivity of the female already present, and/or obliteration of a few eggs caused by the host's tissue reaction produced by the host's

Table 2. Effect of the *A. excelsa* leaf extract (200 and 500 mg/kg/day for 5 days) on worm load in *S. mansoni*-infected mice sacrificed 2 weeks after treatment compared to PZQ.

Groups	Worm load			
	Liver	Portomesenteric	Total worms	Percent worm Reduction%
	Total couples	Total couples		
Infected control	0.80 ± 0.49	5.60 ± 0.60	18.40 ± 0.68	—
PZQ (200 mg/kg)	0.00 ± 0.00*	0.00 ± 0.00**	1.20 ± 0.37**	93.47
Ailanthus excelsa (200 mg/kg)	0.67 ± 0.22*	0.67 ± 0.33**	12.33 ± 1.36**	33.20
Ailanthus excelsa (500 mg/kg)	0.00 ± 0.00*	3.60 ± 0.60**	10.80 ± 0.92**	41.30

PZQ and *A. excelsa* leaf extract were administered orally 7 weeks after *S. mansoni* infection.
Results are presented as mean ± standard error of mean (SEM).
**Significant difference from infected control at $p < 0.01$.
*Significant difference from infected control at $p < 0.05$.

Table 3. Effect of PZQ and *A. excelsa* leaf extract (200 and 500 mg/kg/day for 5 days) on tissue egg load and percentage of egg developmental stages in *S. mansoni*-infected mice sacrificed 2 weeks after treatment.

Groups	Tissue egg load ×10³		% of egg developmental stages		
	Hepatic count	Intestinal count	Immature	Mature	Dead
Infected control	10.94 ± 911.3	17.82 ± 2024.6	57.4 ± 3.89	36.20 ± 3.59	6.40 ± 0.60
PZQ (200 mg/kg)	5.65 ± 0.73**	3.77 ± 0.55**	0.00 ± 0.00**	4.60 ± 2.04**	95.4 ± 2.04**
Ailanthus excelsa (200 mg/kg)	8.92 ± 1.12*	9.22 ± 0.91*	33.00 ± 2.45**	44.16 ± 2.71	22.83 ± 1.92
Ailanthus excelsa (500 mg/kg)	7.79 ± 1.32*	6.36 ± 1.12**	34.00 ± 4.00**	44.00 ± 5.34	22.00 ± 2.55

PZQ and *A. excelsa* leaf extract were administered orally 7 weeks after *S. mansoni* infection.
Results are presented as mean ± SEM.
* Significant difference from infected control at $p < 0.05$.
** Significant difference from infected control at $p < 0.01$.

Table 4. Hepatic granuloma sizes in *S. mansoni*-infected mice treated with PZQ and *A. excelsa* leaf extract (200 and 500 mg/kg/day for 5 days) versus untreated control animals.

Group	Granuloma					Worm
	Egg					
	Number (N/5 high-power field)	Type	Diameter (µm)	Fibrosis (area µm²/LPF)	Inflammation	
Control	29	Fibrocellular 90% Cellular 10%	422.3 ± 66.52	169.83 ± 12.6	Mono++ Neutro+++	NIL
PZQ	12	Fibrocellular 95% Cellular 5%	285.18 ± 56.14**	134.47 ± 54.55**	Mono++ Neutro+++	+++
200	24	Fibrocellular 90% Cellular 10%	389.48 ± 138.92##$	163.68 ± 10.74$	Mono++ Neutro+++	NIL
500	23	Fibrocellular 95% Cellular 5%	277.88 ± 64.54**	149.51 ± 45.75*	Mono++ Neutro+++	NIL

**: Sig. difference from the control group ($p < 0.01$).
*: Sig. difference from the control group ($p < 0.05$).
##: Sig. difference from the 200 group ($p < 0.01$).
$: Sig. difference from the PZQ group ($p < 0.05$).

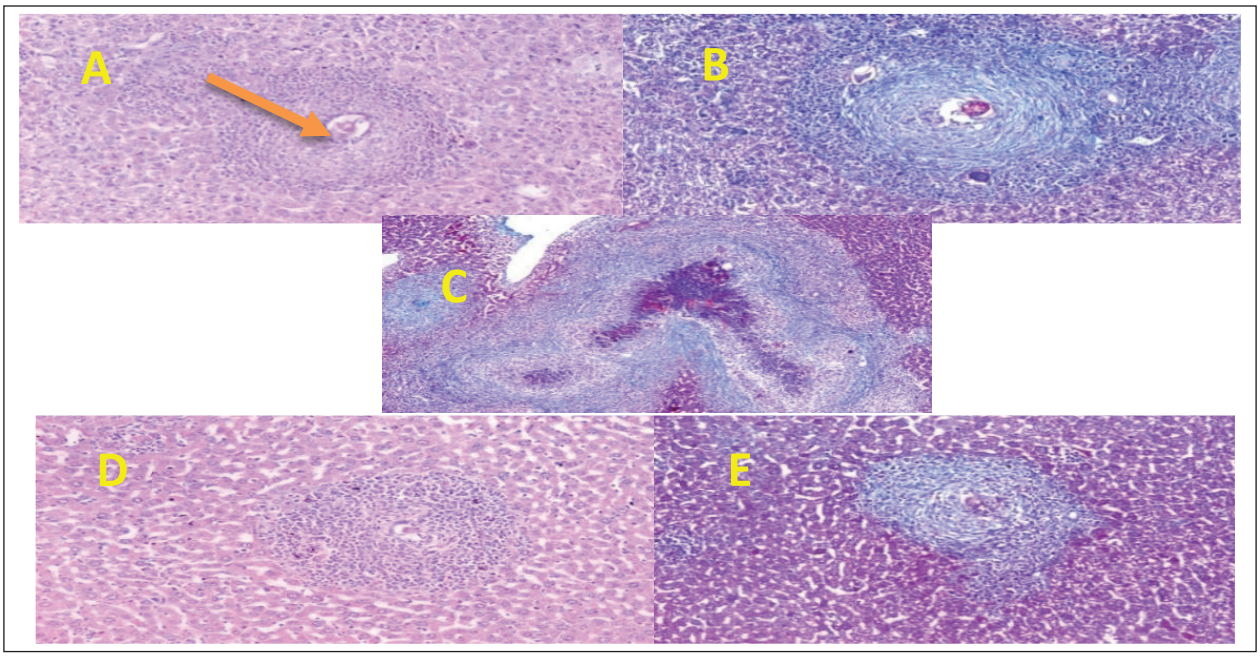

Figure 2. Section in mouse livers of the diverse groups assessed. (A) Control group showing an egg granuloma with central intact ova showing a fibrocellular egg granuloma with central ova and peripheral condensation of neutrophils and concentric layers of fibrous tissue [hematoxylin/eosin (H&E) stain, ×200]. (B) A fibrocellular egg granuloma with central intact ova and concentric layers of fibrous tissue (green color) (MT stain, ×200). (C) PZQ-treated group showing a large dead worm granuloma with marked tissue fibrosis (MT stain, ×50). (D) PZQ-treated group showing a cellular egg granuloma consisting mostly of neutrophils and mononuclear cells (H&E stain, ×200). (E) PZQ-treated group showing a fibrocellular egg granuloma (MT stain, ×200).

tissue reaction. In the current work, data revealed the reduction in tissue egg load in the mice treated with the *A. excelsa* extract was coupled with a significant increase in the percentage of mature and dead eggs for *A. excelsa* compared with the infected untreated mice. These results agree with those of Pellizgo *et al*. (1962), who stated that the absence of immature eggs in the oogram pattern is a significant indicator of drug efficacy. The antioxidants β-carotene and N-acetylcysteine increased the reduction in the total number of worms and tissue egg loads, while increasing the percentage of dead ova and decreasing the percentage of mature ova phases (Ebeid *et al*., 2007; Seif el-Din *et al*., 2006). Histopathological examination of the liver sections in the different studied mice groups showed an enormous number of egg granulomas of large sizes and irregular outlines, with a high percentage of newly formed cellular granulomas. This was in accordance with the results of El-Nahal *et al*. (1998). Otherwise, the PZQ-treated group exhibited a considerable decrease in both egg granulomas' number and diameter, with more regular outlines and higher percentages of fibrocellular granulomas. Many large worm granulomas were detected in the liver sections of this group due to the shift of dead worms from the portal circulation to the liver (El-Lakkany *et al*., 2012). No significant reduction in granuloma count was detected

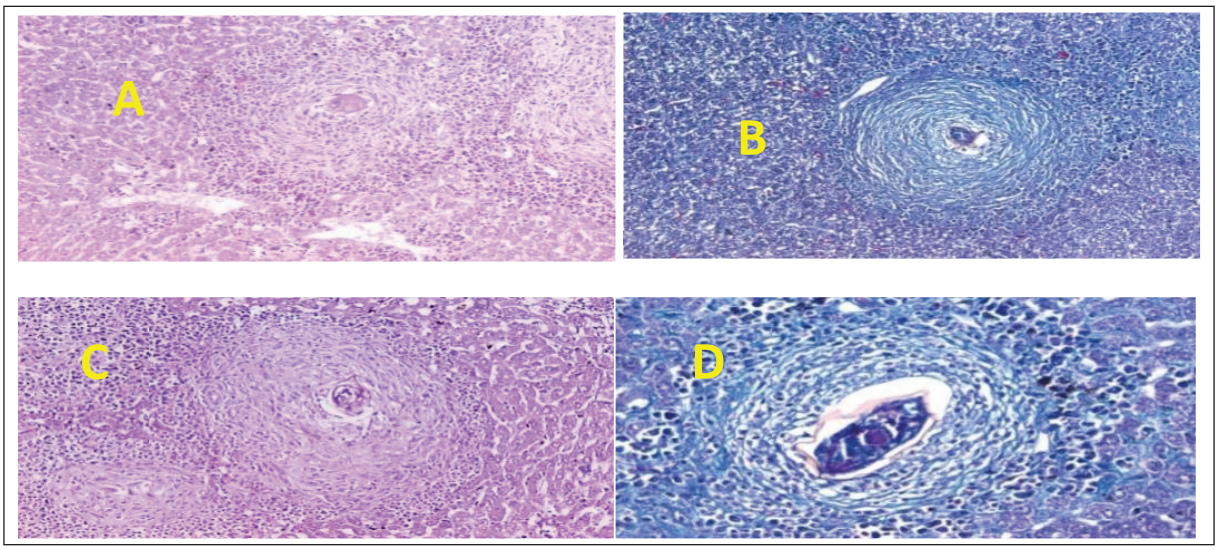

Figure 3. Section in mouse livers of the diverse groups assessed. (A) 200 mg treated group showing an egg granuloma with central intact ova (H&E stain, ×200). (B) 200 mg treated group showing a fibrocellular egg granuloma with central intact ova surrounded by concentric layers of fibrous tissue (green) and peripheral inflammatory cells (MT stain, ×200). (C) 500 mg treated group showing an egg granuloma with central intact ova surrounded by fibrocellular tissue reaction (H&E stain, ×200). (D) 500 mg treated group showing an egg granuloma with a central intact granuloma surrounded by fibrous tissue (green) and peripheral mono- and polymorph nuclear inflammatory cells (MT stain, ×200).

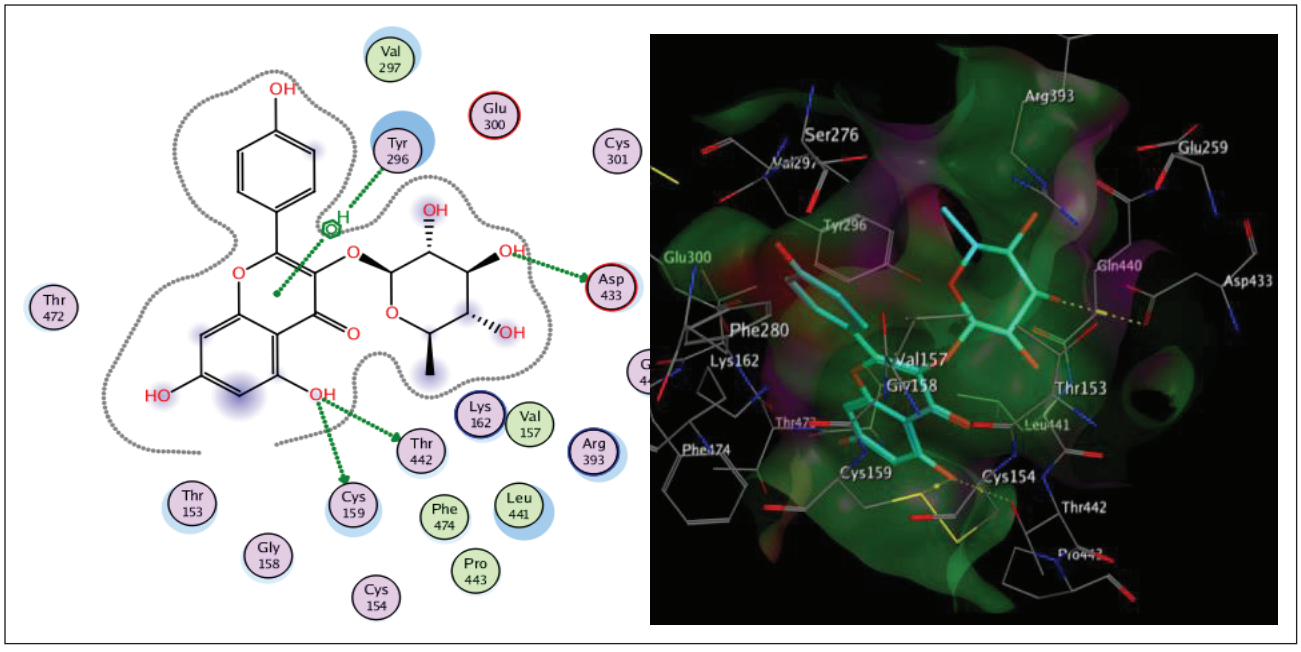

Figure 4. The two-dimensional and three-dimensional suggested binding modes of kaempferin inside the active binding site of TGR.

between the control and the treated groups at both examined doses (200 and 500 mg/kg). This observation pointed to the weak effect of the *A. excelsa* extract in decreasing the number of living worms or their oviposition in both examined doses.

As regards the granuloma diameter, there was a significant reduction in granuloma size in the PZQ- and *A. excelsa*-treated groups (500 mg/kg) relative to the control group. No considerable variation in granuloma diameter was detected between the control and *A. excelsa*-treated group (200 mg/kg). Conversely, a considerable decrease in the mean granuloma diameter was detected at the high dose of the *A. excelsa* extract compared to the control-infected group. This could be attributed to an anti-inflammatory effect of the tested extract, especially at higher doses, resulting in a decrease in the inflammatory pool of each granuloma with a consequent decrease in size. This study sheds light on the *in vivo* antischistosomal potential of the *A. excelsa* extract.

Molecular docking study

Schistosoma mansoni's reliance on TGR to protect itself from expected oxidative stress makes it an attractive therapeutic target (Sharma *et al*., 2009). The skeleton of TGR from *S. mansoni*

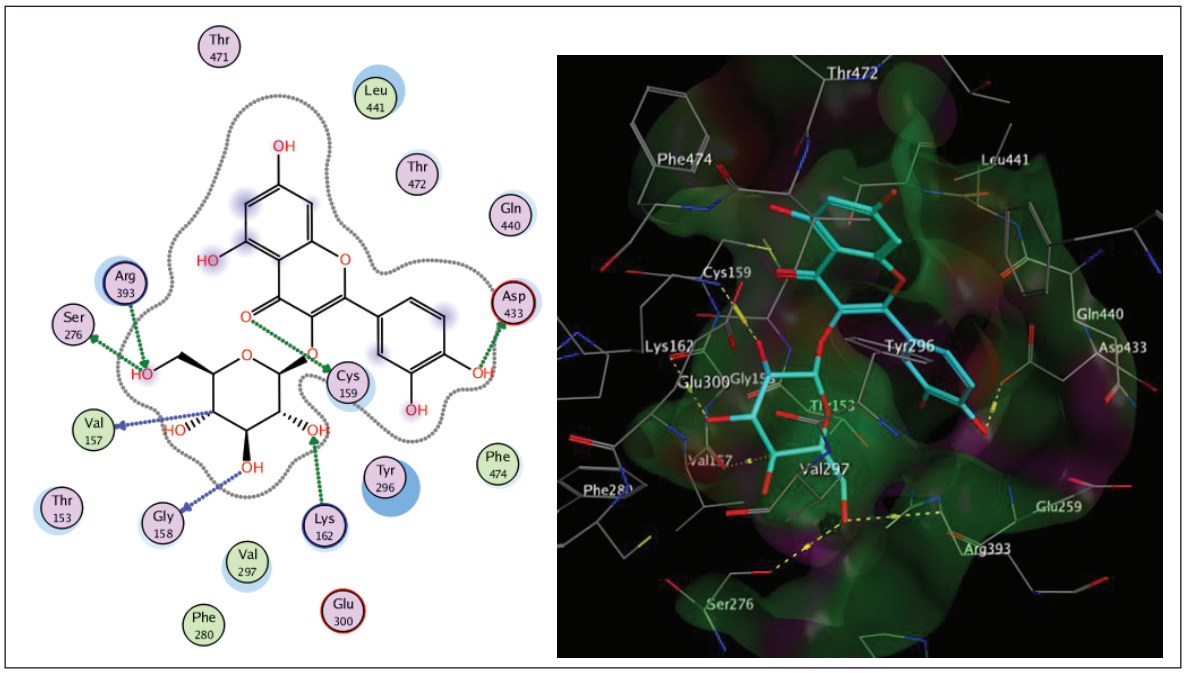

Figure 5. The two-dimensional and three-dimensional suggested binding modes of isoquercitrin inside the active binding site of TGR.

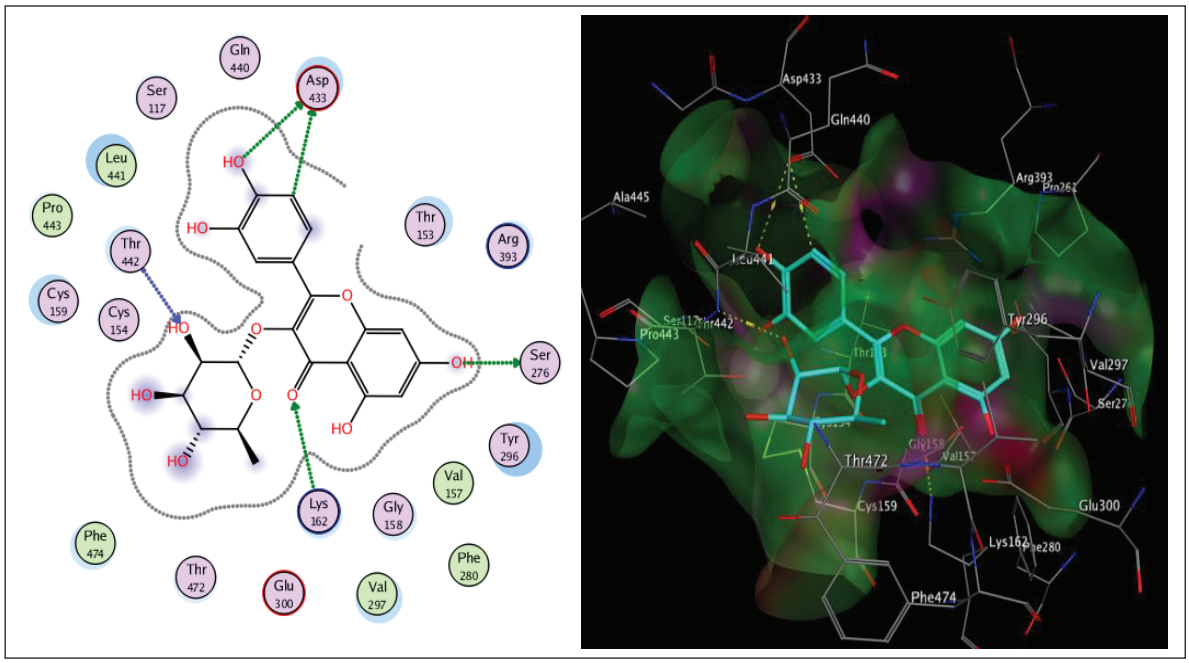

Figure 6. The two-dimensional and three-dimensional suggested binding modes of quercitrin inside the active binding site of TGR.

was found as a fusion of two domains: Grx (1-106) and TR (107-598) (Angelucci *et al*., 2010; Huang *et al*., 2015). Based on the abovementioned findings, we decided to perform a molecular docking study of the five isolated compounds inside the active site of TGR comparing the results with the reference drug PZQ. Herein, a molecular docking study was done to predict and score the poses of the ligand–protein binding. The docking studies were performed using MOE 2014.0901. The TGR crystal structure was downloaded from a protein data bank (PDB:2V6O). The results are shown in Figures 4–7 and Table 1S and Figures 2S and 3S. PZQ revealed a docking score of −6.407 kcal/mol showing two hydrogen bonds with Cys159 and Thr442. The least binding scores were observed for compounds gallic acid and methyl gallate displaying binding energies of −3.278 and −4.718, respectively. Kaempferol-3-*O*-rhamnoside was able to fit inside the pocket by forming three hydrogen bonds with Asp433, Cys159, and Thr442, besides one arene-H interaction with Tyr296, revealing a binding score of −8.758 kcal/mol. Also quercitrin was bounded via four hydrogen bonds with the Asp433, Lys162, Thr442, and Ser276 amino acids, whereas isoquercitrin among all compounds

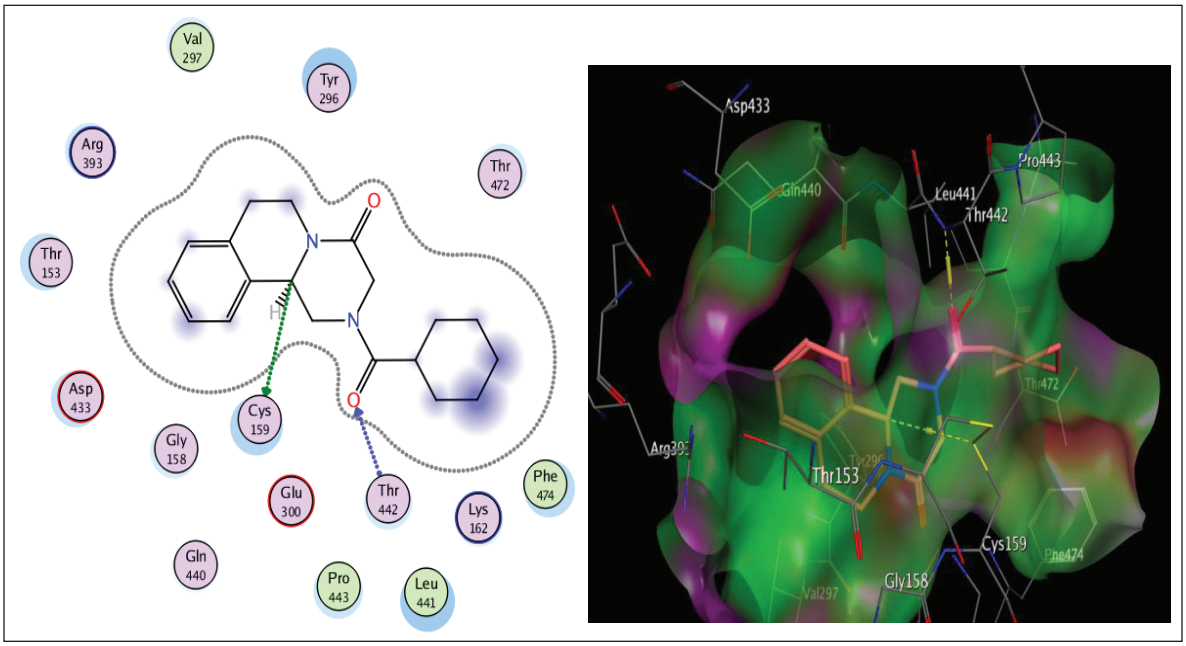

Figure 7. The two-dimensional and three-dimensional suggested binding modes of PZQ inside the active binding site of TGR.

displayed seven H- bonds with the most important amino acids inside the active site with an energy score of −11.370 kcal/mol.

CONCLUSION

The *A. excelsa* leaf extract has a high concentration of polyphenolic metabolites, which have been tentatively identified by LC-ESI-MS/MS and characterized as antischistosomal. The current investigation found a significant reduction in the number of worms and eggs after treatment with the plant extract. Therefore, the plant is considered a strong candidate as a promising source of natural antischistosomiasis agents**.**

LIST OF ABBREVIATIONS

^{13}C-NMR: Carbon-13 magnetic resonance; DMSO: Dimethyl sulfoxide; Grx: Glutaredoxin; H&E: Hematoxylin/eosin; ^{1}H-NMR: Proton magnetic resonance; LPF: Low-power field; LC-ESI-MS/MS: Liquid chromatography-electrospray ionization tandem/mass spectrometry; LPF: Low-power field; MHz: Megahertz; MOE: Molecular Operating Environment; PC: Paper chromatography; PZQ: Praziquantel; SEM: Standard error of mean; TGR: Thioredoxin glutathione reductase; TR: Thioredoxin reductase;

CONFLICT OF INTEREST

No potential conflicts of interest were reported by the authors.

FUNDING

There is no funding to report.

ETHICAL APPROVAL

All the experiments on animals were conducted according to the internationally valid guidelines after the approval of the Institutional Theodor Bilharz Research Institute-Research Ethical Committee (TBRI-REC). The serial number of the protocol is PT (606).

AUTHORS' CONTRIBUTIONS

HSM and MAG conceived and designed the experiments; searched for information; performed extraction, fractionation, chromatographic isolation, structural elucidation, and LC-ESI-MS/MS interpretation; drafted the original paper; and revised the last version. SW evaluated in vivo antischistosomal activity. TA performed the histopathological examination. HA performed the statistical analysis. RS performed the molecular docking experiment. All authors contributed to manuscript revision and read and approved the submitted version.

DATA AVAILABILITY

All the data obtained during the study are presented in this manuscript. Any further inquiries for additional information are available upon request from the corresponding author.

PUBLISHER'S NOTE

This journal remains neutral with regard to jurisdictional claims in published institutional affiliation.

REFERENCES

Adamik K, Brauns FE. *Ailanthus glandulosa* (tree-of-heaven) as a pulpwood. TAPPI, 1957; 40:522–7.

Agrawal PK. In carbon-13 NMR of flavonoids. Carbon-13 NMR of flavonoids: studies in organic chemistry series. In: Agrawal PK (ed.). Elsevier, New York, NY, pp 450–3, 1989.

Alger HM, Williams DL. The disulfide redox system of *Schistosoma mansoni* and the importance of a multifunctional enzyme, thioredoxin glutathione reductase. Mol Biochem Parasitol, 2002; 121:129–39.

Ammar S, Contreras MDM, Belguith-Hadrich O, Bouaziz M, Segura-Carretero A. New insights into the qualitative phenolic profile of *Ficus carica* L. fruits and leaves from Tunisia using ultra-high-performance liquid chromatography coupled to quadrupole-time-of-flight mass spectrometry and their antioxidant activity. RSC Adv, 2015; 5:20035–50.

Andrews P. Praziquantel: mechanisms of anti-schistosomal activity. Pharmacol Ther, 1985; 29(1):129–56.

Angelucci F, Dimastrogiovanni D, Boumis G, Brunori M, Miele AE, Saccoccia F, Bellelli A. Mapping the catalytic cycle of *Schistosoma mansoni* thioredoxin glutathione reductase by X-ray crystallography. J Biol Chem, 2010; 285:32557–67.

Asolkar LV, Kakkar KK, Chakre OJ. Glossary of Indian medicinal plants with active principles. C.S.I.R., New Delhi, India, pp 34–58, 1992.

Bakchiche B, Gherib A, Bronze MR, Ghareeb MA. Identification, quantification, and antioxidant activity of hydroalcoholic extract of *Artemisia campestris* from Algeria. Turkish J Pharm Sci, 2019; 16(2):234–9.

Barros L, Dueňas M, Ferreira ICFR, Carvalho AM, Santos-Buelga C. Use of HPLC–DAD-ESI/MS to profile phenolic compounds in edible wild greens from Portugal. Food Chem, 2011; 127:1690173.

British Pharmacopoeia. II. H. M. Stationary office. British Pharmacopoeia, London, UK, 704 p, 1988.

Cabrera W, Genta S, Said A, Farag A, Rashed K, Sánchez S. Hypoglycemic activity of *Ailanthus excelsa* leaves in normal and streptozotocin-induced diabetic rats. Phytother Res, 2008; 22(3):303–7.

Chanda J, Mukherjee PK, Biswas R, Biswas S, Tiwari AK, Pargaonkar A. UPLC-QTOF-MS analysis of a carbonic anhydrase-inhibiting extract and fractions of *Luffa acutangula* (L.) Roxb (ridge gourd). Phytochem Anal, 2019; 30:148–55.

Chauhan K, Santwani P, Parmar L, Solanki R, Adeshara S. Evaluation of antidepressant activity of *Ailanthus excelsa* Roxb. using mice as experimental animal. Res J Pahrmacol Pharmacodyn, 2011; 3(3):102–4.

Chevellier A. The encyclopedia of medicinal plants, a practical reference guide. Kindersley Dorling Ltd, London, UK, pp 74–80, 1996.

Choi JG, Mun SH, Chahar HS, Bharaj P, Kang OH, Kim SG, Shin DW, Kwon DY. Methyl gallate from *Galla rhois* successfully controls clinical isolates of Salmonella infection in both *in vitro* and *in vivo* systems. PLoS One, 2014; 9(7):e102697.

Dash SK, Padhy S. Review on ethnomedicines for diarrhoea diseases from Orissa. J Hum Ecol, 2006, 20(1):59–64.

Doenhoff MJ, Cioli D, Utzinger J. Praziquantel: mechanisms of action, resistance, and new derivatives for schistosomiasis. Curr Opin Infect Dis, 2008; 21:659–67.

Duvall RH, DeWitt WB. An improved perfusion technique for recovering adult schistosomes from laboratory animals. Am J Trop Med Hyg, 1967; 16:483–6.

Ebeid FA, Ezzat AR, Badawy AA, Seif el-Din SH. Enhancement role of β-carotene against experimental schistosomiasis. Egypt J Schistosomiasis Infect Endem Dis, 2007; 29:67–90.

Eldahshan OA. Isolation and structure elucidation of phenolic compounds of Carob leaves grown in Egypt. Curr Res J Biol Sci, 2011; 3(1):52–5.

El-Lakkany N, Hammam O, El-Maadawy W, Badawy A, Ain-Shoka A, Ebeid F. Anti-inflammatory/anti-fibrotic effects of the hepatoprotective silymarin and the schistosomicide praziquantel against *Schistosoma mansoni*-induced liver fibrosis. Parasit Vectors, 2012; 5(9):1–14.

El-Nahal HM, Kaddah MA, Hassan SI, Abdel Ghany A, Ibrahim AM, Ramzy RM, Mostafa EA. Effect of *Schistosoma mansoni* infection on offsprings born from infected mothers. J Egypt Soc Parasitol, 1998; 28(2):523–38.

El-Sayed MM, Mahmoud MA, El-Nahas HA, El-Toumy SA, El-Wakil EA. Ghareeb MA. Chemical constituents, antischistosomal and antioxidant activity of methanol extract of *Azadirachta indica*. Egypt J Chem, 2011; 54:105–19.

Fallon PG, Doenhoff MJ. Drug-resistant schistosomiasis: resistance to praziquantel and oxamniquine induced in *Schistosoma mansoni* in mice is drug specific. Am J Trop Med Hyg, 1994; 51:83–8.

Ghareeb MA, Mohamed T, Saad AM, Refahy LA, Sobeh M, Wink M. HPLC-DAD-ESI-MS/MS analysis of fruits from *Firmiana simplex* (L.) and evaluation of their antioxidant and antigenotoxic properties. J Pharm Pharmacol, 2018b; 70:133–42.

Ghareeb MA, Saad AM, Ahmed WS, Refahy LA, Nasr SM. HPLC-DAD-ESI-MS/MS characterization of bioactive secondary metabolites from *Strelitzia nicolai* leaf extracts and their antioxidant and anticancer activities *in vitro*. Pharmacogn Res, 2018c; 10(4):368–78.

Ghareeb MA, Sobeh M, El-Maadawy WH, Mohammed HS, Khalil H, Botros SS, Wink M. Chemical profiling of polyphenolics in *Eucalyptus globulus* and evaluation of its hepato-renal protective potential against cyclophosphamide induced toxicity in mice. Antioxidants, 2019; 8(9):415.

Ghareeb MA, Sobeh M, Rezq S, El-Shazly AM, Mahmoud MF, Wink M. HPLC-ESI-MS/MS profiling of polyphenolics of a leaf extract from *Alpinia zerumbet* (Zingiberaceae) and its anti-inflammatory, anti-nociceptive, and antipyretic activities *in vivo*. Molecules, 2018a; 23:3238.

Ghumare P, Jirekar DB, Farooqui M, Naikwade SD. Physico-chemical, phytochemical screening, and antimicrobial activity of *Ailanthus excelsa* leaves. Int J Chem Sci, 2014; 12(4):1221–30.

Gönnert R, Andrews P. Praziquantel, a new board-spectrum antischistosomal agent. Z Parsitenkd, 1977; 52:129–50.

Goufo P, Singh RK, Cortez I. A reference list of phenolic compounds (including stilbenes) in grapevine (*Vitis vinifera* L.) roots, woods, canes, stems, and leaves. Antioxidants, 2020; 9:398.

Gray DJ, Ross AG, Li YS, McManus DP. Diagnosis and management of schistosomiasis. BMJ, 2011; 342:d2651.

Harborne JB, Mabry TJ. The flavonoids advances in research. Chapman and Hall, London, UK; New York, NY, 1982.

Hotez PJ, Kamath, A. Neglected tropical diseases in sub-Saharan Africa: review of their prevalence, distribution, and disease burden. PLoS Negl Trop Dis, 2009; 3:e412.

Huang J, Hua W, Li J, Hua Z. Molecular docking to explore the possible binding mode of potential inhibitors of thioredoxin glutathione reductase. Mol Med Rep. 2015; 12:5787–95.

Hukkeri VI, Jaiprakash B, Lavhale MS, Karadi RV, Kuppast IJ. Hepatoprotective activity of *Ailanthus excelsa* Roxb. Leaf extract on experimental liver damage in rats. Indian J Pharm Educ, 2002; 37:105–6.

Ibrahim AM, Hussein TM, Abdel-Tawab H, Hammam OA, Ghareeb MA. The ameliorative effects of *Eremina desertorum* snail mucin in combination with Silymarin against experimentally induced liver fibrosis. Egypt J Chem, 2022**;** 65(2):181–90.

Ismail MM, Taha SA, Farghaly AM, El-Azony AS. Laboratory induced resistance to praziquantel in experimental schistosomiasis. J Egypt Soc Parasitol, 1994; 24:685–95.

Joshi BC, Pandey A, Sharma RP, Khare A. Quassinoids from *Ailanthus excelsa*. Phytochemistry, 2003: 62:579–84

Kamel IA, Cheever AW, Elwi AM, Mosimann JE, Danner R. *Schistosoma mansoni* and S. *haematobium* infections in Egypt: technique for recovery of worms at necropsy. Am J Trop Med Hyg, 1977; 26(4):696–701.

Kapoor SK, Ahmad PI, Zaman A. Simarubaceae chemical constituents of *Ailanthus excelsa*. Phytochemistry, 1971; 10(12):3333.

Khushbu C, Lalkrushn P, Roshni S, Dhruvil S, Adeshara SP. Evaluation of analgesic activity of *Ailanthus excelsa* Roxb. using rat as an experimental animal. J Pharm Res, 2011; 4(5):1336.

Kirtikar KR, Basu BD. Indian medicinal plants. International Books Distributor, Dehradun, India, vol. 1, pp 505–7, 1995.

Kumar D, Bhujbal SS, Deoda RS, Mudgade SC. *In-vitro* and *in-vivo* antiasthmatic studies of *Ailanthus excelsa* Roxb. on Guinea pigs. J Sci Res, 2010; 2(1):196–202.

Kumar S, Singh A, Kumar B. Identification, and characterization of phenolics and terpenoids from ethanolic extracts of *Phyllanthus* species by HPLC-ESI-QTOF-MS/MS. J Pharm Anal, 2017; 7:214–22.

Kuntz AN, Davioud CE, Sayed AA, Califf LL, Dessolin J, Arne´r ES, Williams DL. Thioredoxin glutathione reductase from *Schistosoma mansoni*: an essential parasite enzyme and a key drug target. PLoS Med, 2007; 4e206:1071–86.

Li A, Hou X, Wei Y. Fast screening of flavonoids from switch grass and *Mikania micrantha* by liquid chromatography hybrid-ion trap time-of-flight mass spectrometry. Anal Meth, 2018; 10:109.

Liang YS, John BI, Boyd DA. Laboratory cultivation of schistosome vector snails and maintenance of schistosome life cycles. Proceed 1st Sino-American Symp. 1987; 1:34–48.

Loizzo MR, Said A, Tundis R, Rashed K, Statti GA, Hufner A, Menichini F. Inhibition of angiotensin converting enzyme (ACE) by flavonoids isolated from *Ailanthus excelsa* (Roxb.) (Simaroubaceae). Phytother Res, 2007; 21:32–6.

Ma X, Wu Y, Li Y, Huang Y, Liu Y, Luo P, Zhang Z. Rapid discrimination of *Notopterygium incisum* and *Notopterygium franchetii* based on characteristic compound profiles detected by UHPLC-QTOF-MS/MS coupled with multivariate analysis. Phytochem Anal, 2020; 31:355–65.

Mabry TJ, Markham KR, Thomas MB. The systematic identification of flavonoids. In: The ultraviolet spectra of flavones and flavonols, Springer, Berlin, Germany, pp 41–164, 1970.

Magana AA, Wright K, Vaswani A, Caruso M, Reed RL, Bailey CF, Nguyen T, Gray NE, Soumyanath A, Quinn J, Stevens JF, Maier CS. Integration of mass spectral fingerprinting analysis with precursor ion (MS1) quantification for the characterisation of botanical extracts: application to extracts of *Centella asiatica* (L.) Urban. Phytochem Anal, 2020; 31:722–38.

Manikandan A, Rajendran R, Balachandar S, Sanumol MS, Sweety MM. Antimicrobial activity of *Ailanthus excelsa* Roxb. collected from Coimbatore district, Tamil Nadu, India. World J Pharm Pharm Sci, 2015; 4(03):697–704.

Mohammed HS, Abdel-Aziz MM, Abu-baker MS, Saad AM, Mohamed MA, Ghareeb MA. Antibacterial and potential antidiabetic activities of flavone C-glycosides isolated from *Beta vulgaris* subspecies cicla L. var. flavescens (Amaranthaceae) cultivated in Egypt. Curr Pharm Biotechnol, 2019; 20(7):595–604.

Molecular Operating Environment (MOE). Chemical Computing Group Inc., Montreal, CA, 2014. Available via http://www.chemcomp.com

Nag A, Matai S. *Ailanthus excelsa* Roxb. (Simaroubaceae), a promising source of leaf protein. J Agric Food Chem, 1994; 35:1115–7.

Nandutu AM, Clifford M, Howell NK. Analysis of phenolic compounds in Ugandan sweet potato varieties (NSP, SPK AND TZ). Afr J Biochem Res, 2007; 1(3):29–36.

Ogura M, Cordell GA, Kinghorn AD, Farnsworth NR. Potential anticancer agents' VI constituents of *Ailanthus excelsa* (Simaroubaceae). Lioydia, 1977; 40:579–84.

Olennikov DN, Chirikova NK, Kashchenko NI, Nikolaev VM, Kim S-W and Vennos C. Bioactive phenolics of the genus *Artemisia* (Asteraceae): HPLC-DAD-ESI-TQ-MS/MS profile of the Siberian species and their inhibitory potential against α-amylase and α-glucosidase. Front Pharmacol, 2018; 9:756.

Pandith JI. Preliminary phytochemical screening and antidermatophytic activity of *Ailanthus excelsa* against human pathogenic fungi. Am J PharmTech Res, 2012; 2(5):423–8.

Pellegrino J, Oliveira CA, Faria J, Cunha AS. New approach to the screening of drugs in experimental schistosomiasis mansoni in mice. Am J Trop Med Hyg, 1962; 11:201–15.

Phillipson JD. Natural products as drugs. Trans R Soc Trop Med Hyg, 1994; 88:17–9.

Rashed K, Said A, Ahmed M. Antiviral activity and phytochemical analysis of *Ailanthus excelsa* Roxb bark. J For Prod Indust, 2013; 2(3):30–3.

Ratha RR, Shamkuwar PB, Pawar DP. Antifungal study of *Ailanthus excelsa* leaves. J Chem Pharm Res, 2013, 5(6):152–4.

Reed KA. Identification of phenolic compounds from peanut skin using HPLC-MSn. Dissertation, Faculty of the Virginia Polytechnic Institute and State University, Blacksburg, VI, 2009.

Said A, Tundis R, Hawas WU, El-Kousy S, Rashed K**,** Menichini F, Bonesi M, Huefner A, Monica RL, Menichini F. *In vitro* antioxidant and antiproliferative activities of flavonoids from *Ailanthus excelsa* (Roxb) (Simaroubaceae) leaves. Z Naturforsch, 2010; 65c:180–6.

Said A., Rashed K., Tokuda H., Huefner A. Antitumor activity of *Ailanthus excelsa* Roxb. stem bark fractions and of canthin-6-one. IUFS J Biol, 2012; 71(1):112–21.

Seif el-Din SH, Ebeid FA, Badawy AA, Ezzat AR. Protective effects of β-carotene; N-acetyl-L-cysteine with and without praziquantel treatment in *Schistosoma mansoni*-infected mice. Egypt J Schistosomiasis Infect Endem Dis, 2006; 28:67–90.

Sharma M, Khanna S, Bulusu G, Mitra A. Comparative modeling of thioredoxin glutathione reductase from Schistosoma mansoni: a multifunctional target for antischistosomal therapy. J Mol Graph Model, 2009; 27:665–75.

Sharma PV, Guna-Vijnana D. Ayurvedic series-III, vegetable drugs. VIIth edition. Chaukhambha Bharati Academy, Varanasi, India, vol. 2, pp 466–68, 1996.

Sherman MM, Borris RP, Ogura M, Cordell GA, Farnsworth NR. 3*S*,24*S*,25-Trihydroxytirucall-7-ene from *Ailanthus excelsa*. Phytochemistry, 1980; 19:1499–501.

Shrimali M, Jain DC, Darokar MP, Sharma RP. Antibacterial activity of *Ailanthus excelsa* (Roxb.). Phytother Res, 2001; 15:165–6.

Simirgiotis MJ, Benites J, Areche C, Sepúlveda B. Antioxidant capacities and analysis of phenolic compounds in three endemic *Nolana* species by HPLC-PDA-ESI-MS. Molecules, 2015; 20:11490–507.

Sobeh M, Mahmoud MF, Hasan RA, Abdelfattah MAO, Sabry OM, Ghareeb MA, El-Shazly AM, Wink M. Tannin-rich extracts from *Lannea stuhlmannii* and *Lannea humilis* (Anacardiaceae) exhibit hepatoprotective activities *in vivo* via enhancement of the anti-apoptotic protein Bcl-2. Sci Rep, 2018; 8:9343.

Šuković D, Knežević B, Gašić U, Sredojević M, Ćirić I, Todić S, Mutić J, Tešić Ž. Phenolic profiles of leaves, grapes, and wine of grapevine variety vranac (*Vitis vinifera* L.) from Montenegro. Foods, 2020; 9:138.

Tasioula-Margari M, Tsabolatidou E. Extraction, separation, and identification of phenolic compounds in virgin olive oil by HPLC-DAD and HPLC-MS. Antioxidants, 2015; 4:548–62.

Wang F, Huang S, Chen Q, Hu Z, Li Z, Zheng P, Liu X, Li S, Zhang S, Chen J. Chemical characterisation and quantification of the major constituents in the Chinese herbal formula Jian-Pi-Yi-Shen pill by UPLC-Q-TOF-MS/MS and HPLC-QQQ-MS/MS. Phytochem Anal, 2020; 31:915–29.

How to cite this article:
Mohammed HS, William S, Aboushousha T, Taleb HMA, Sabour R, Ghareeb MA. *Ailanthus excelsa* leaf extract: Chemical characterization, antischistosomal activity, and *in silico* study of isolated phenolic compounds as promising thioredoxin glutathione reductase inhibitors. J Appl Pharm Sci, 2023; 13(02):124–145.

SUPPLEMENTARY MATERIALS

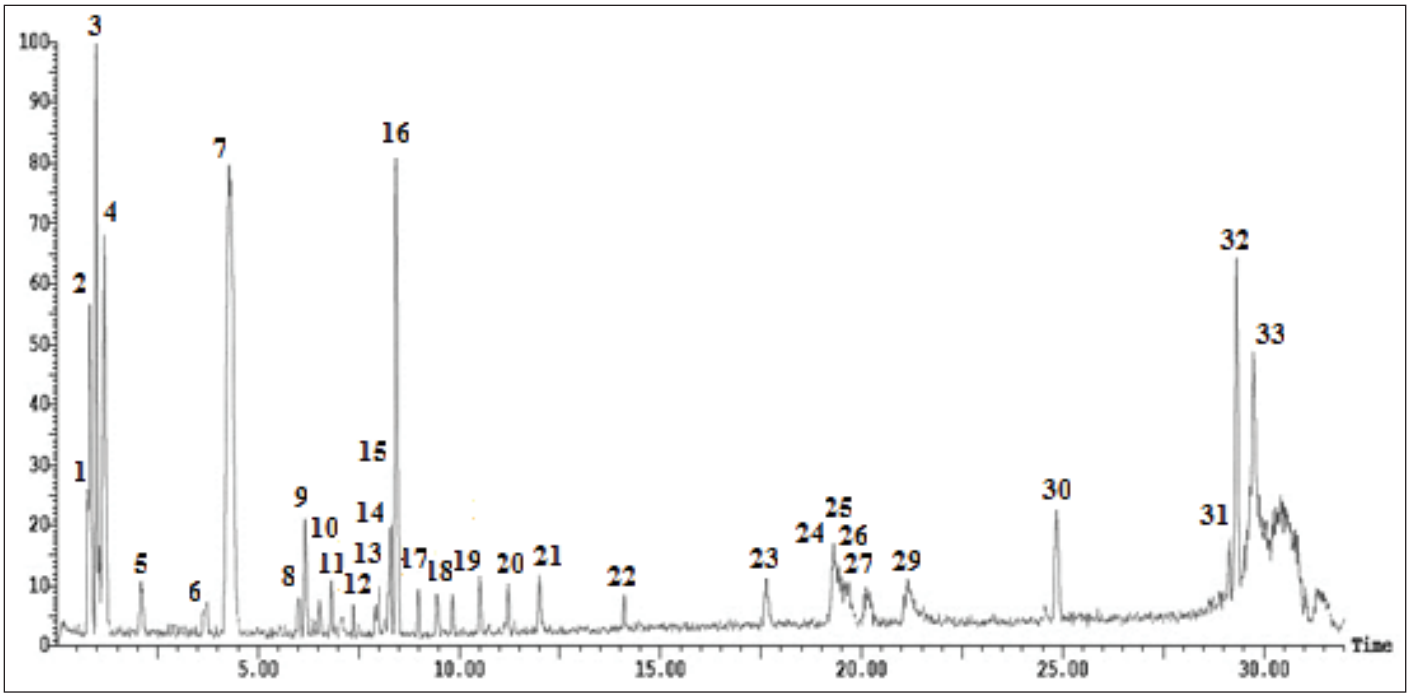

Figure 1S. Negative LC-ESI-MS/MS profile of phenolic compounds from n-butanol extract of A. excelsa leaves.

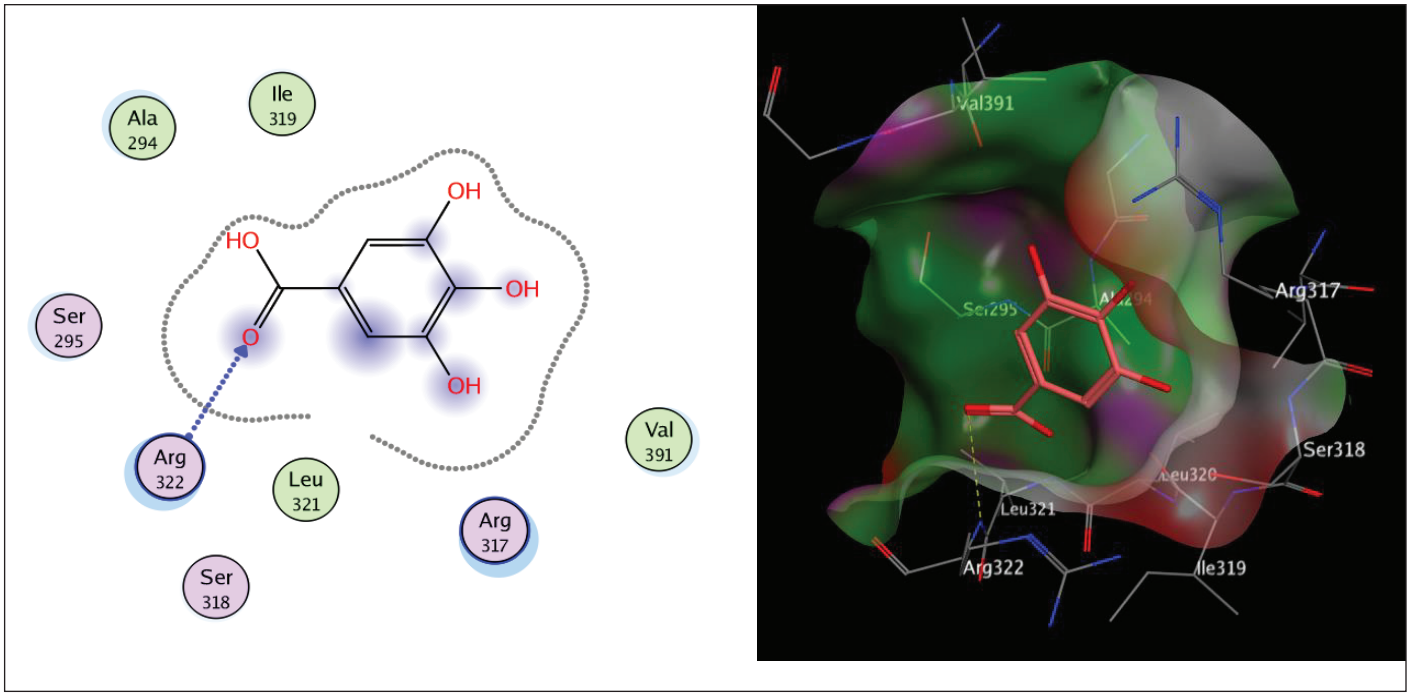

Figure 2S. The two-dimensional and three-dimensional suggested binding modes of Gallic acid inside the active binding site of TGR.

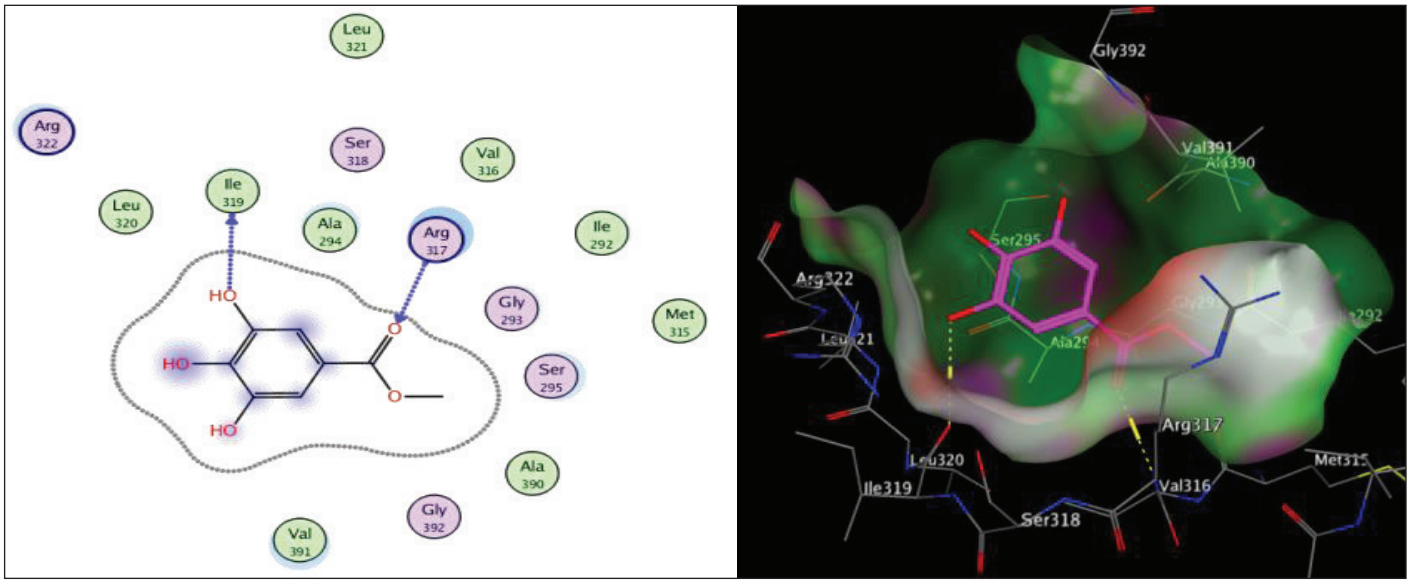

Figure 3S. The two-dimensional and three-dimensional suggested binding modes of Methyl gallate inside the active binding site of TGR.

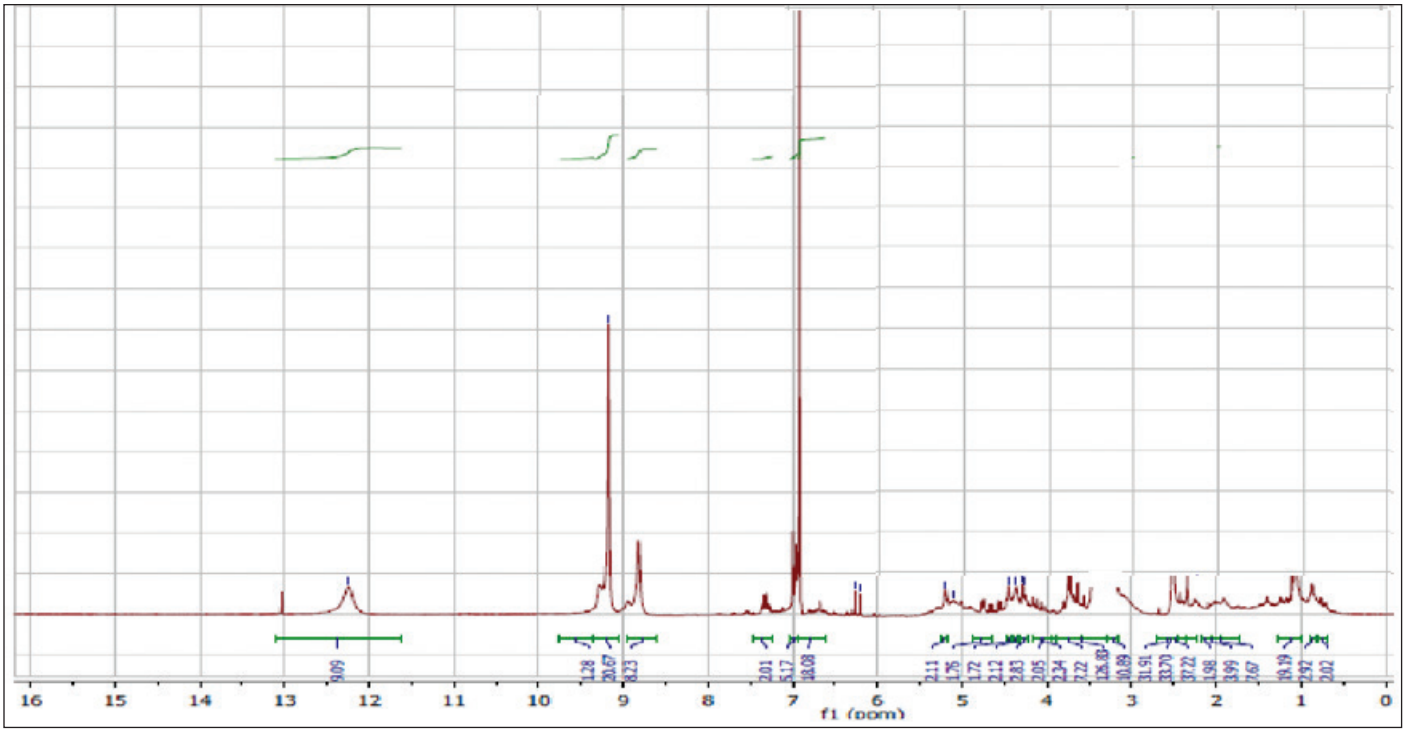

Figure 4S. ^{1}H-NMR spectra of gallic acid.

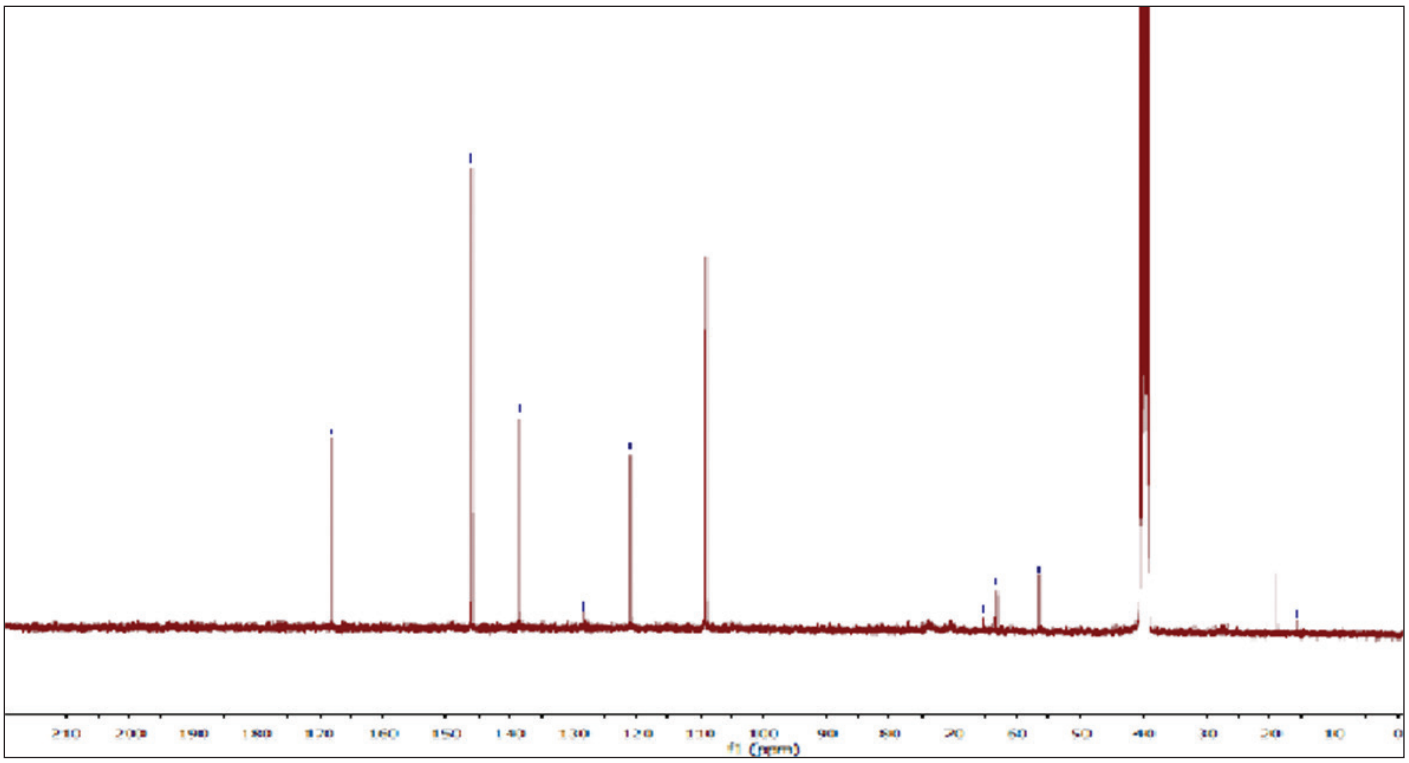

Figure 5S. [13]C-NMR spectra of gallic acid.

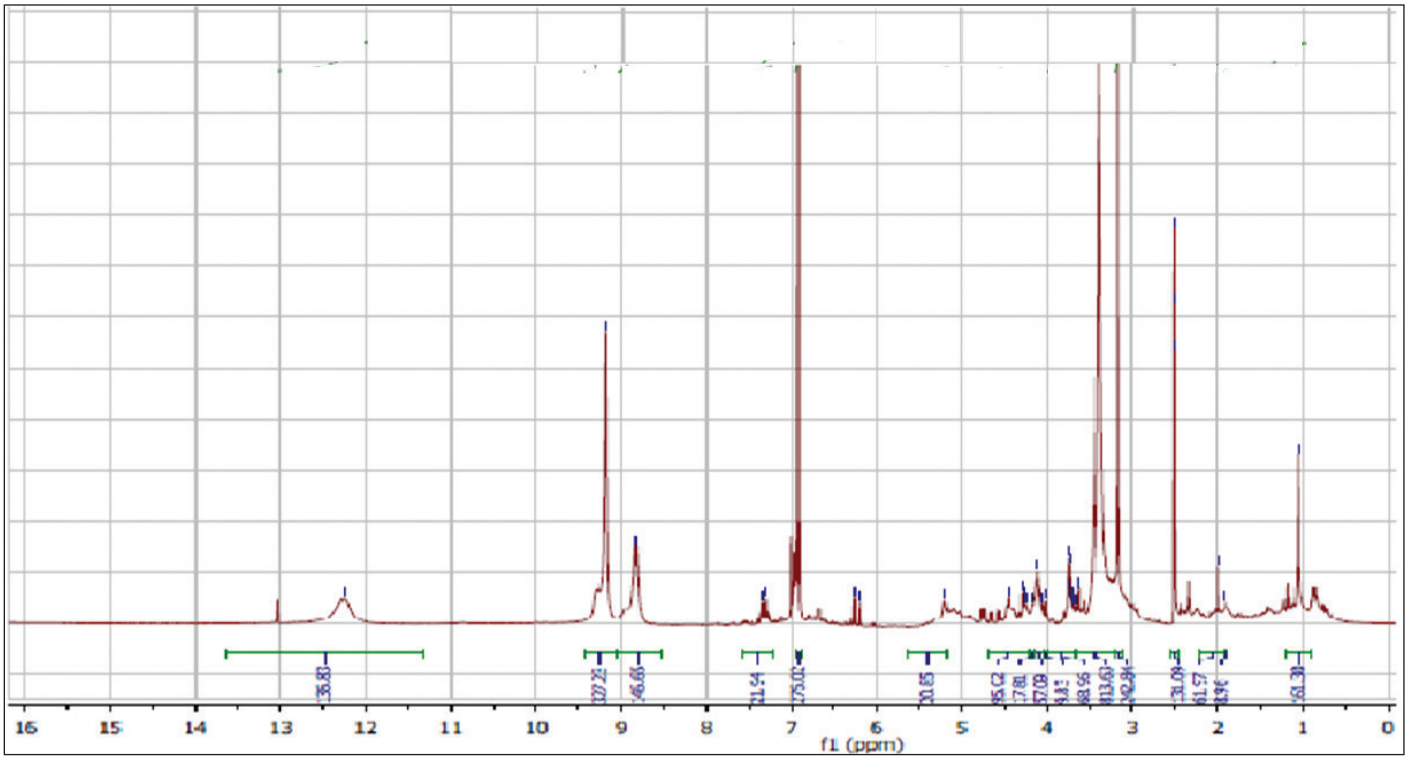

Figure 6S. [1]H-NMR spectra of methyl gallate.

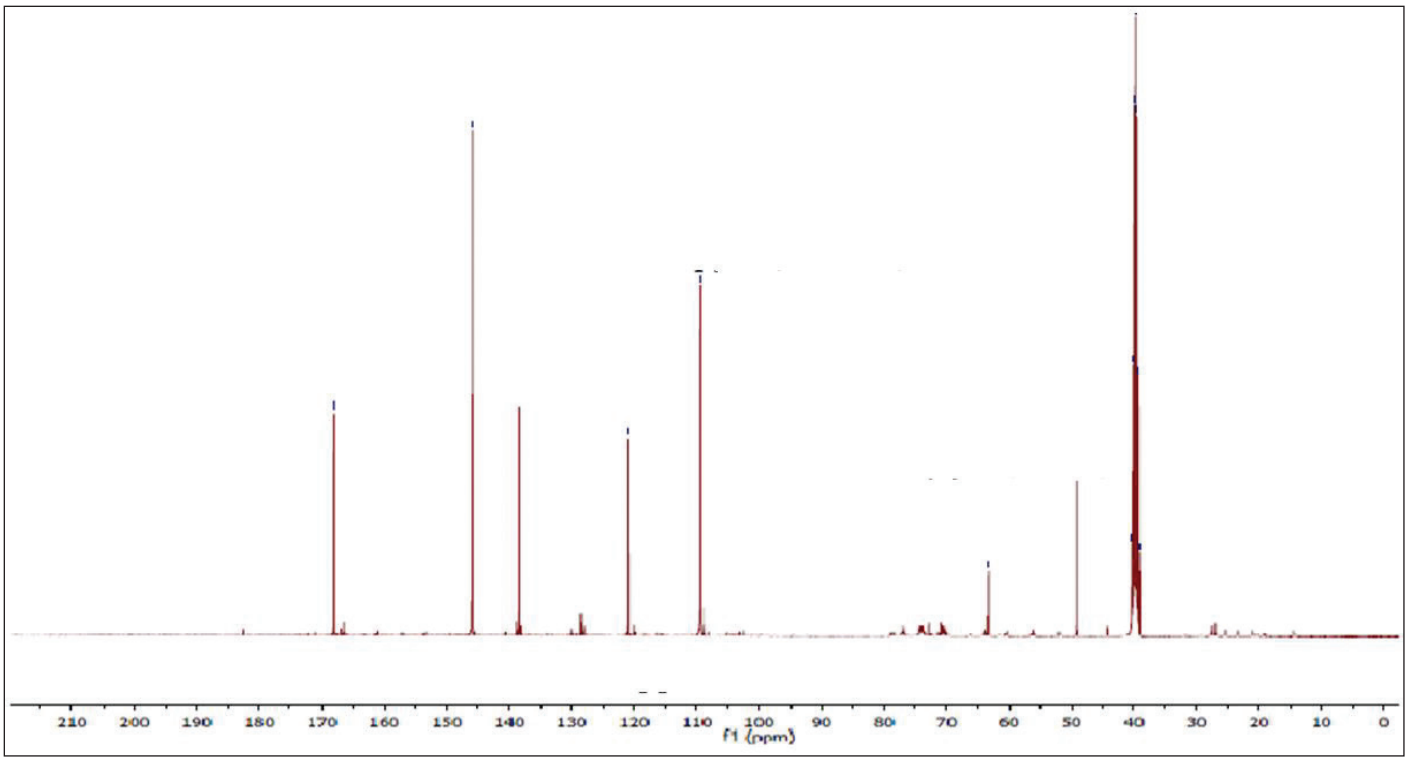

Figure 7S. [13]C-NMR spectra of methyl gallate.

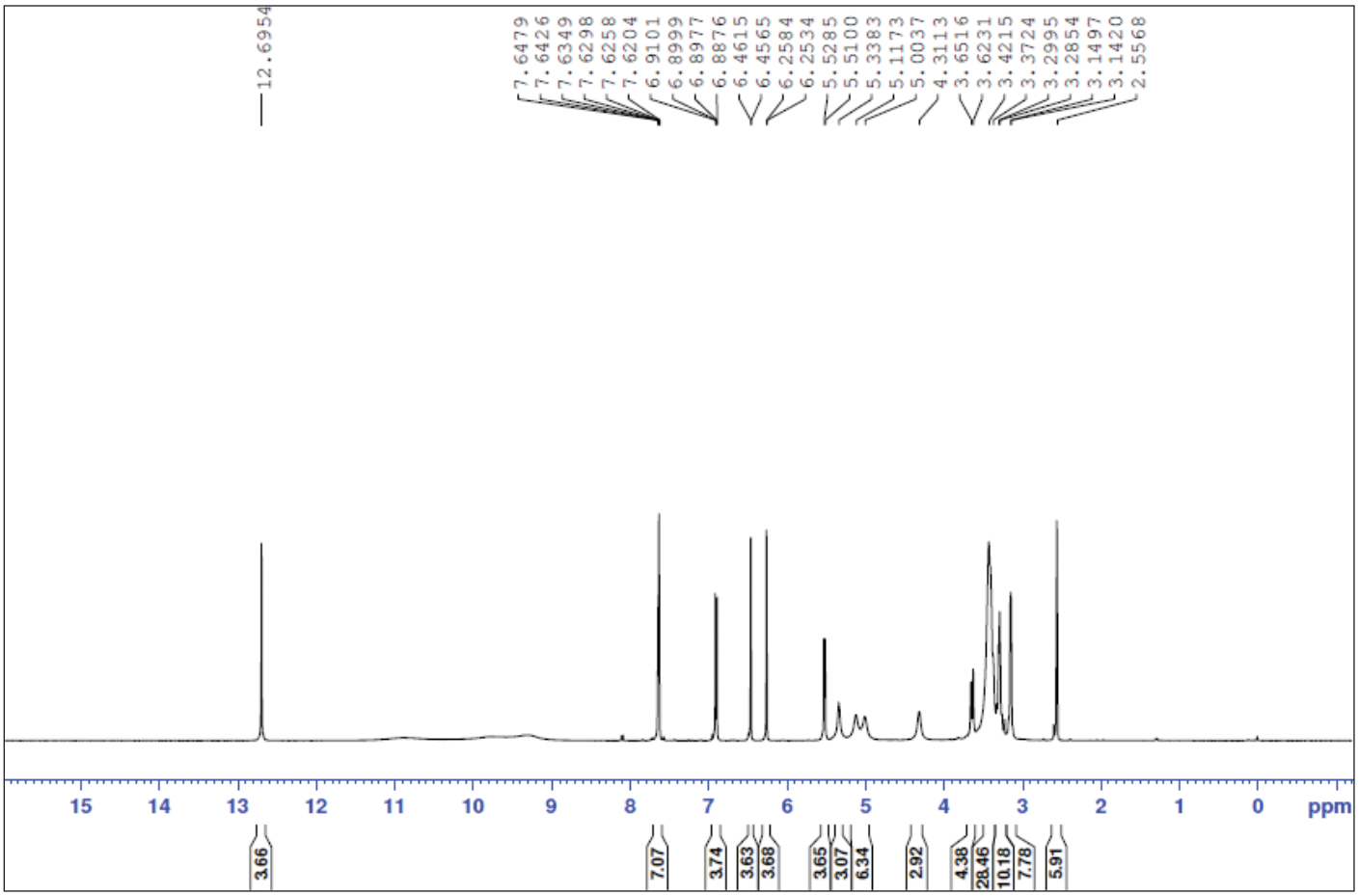

Figure 8S. [1]H-NMR spectra of isoquercitrin.

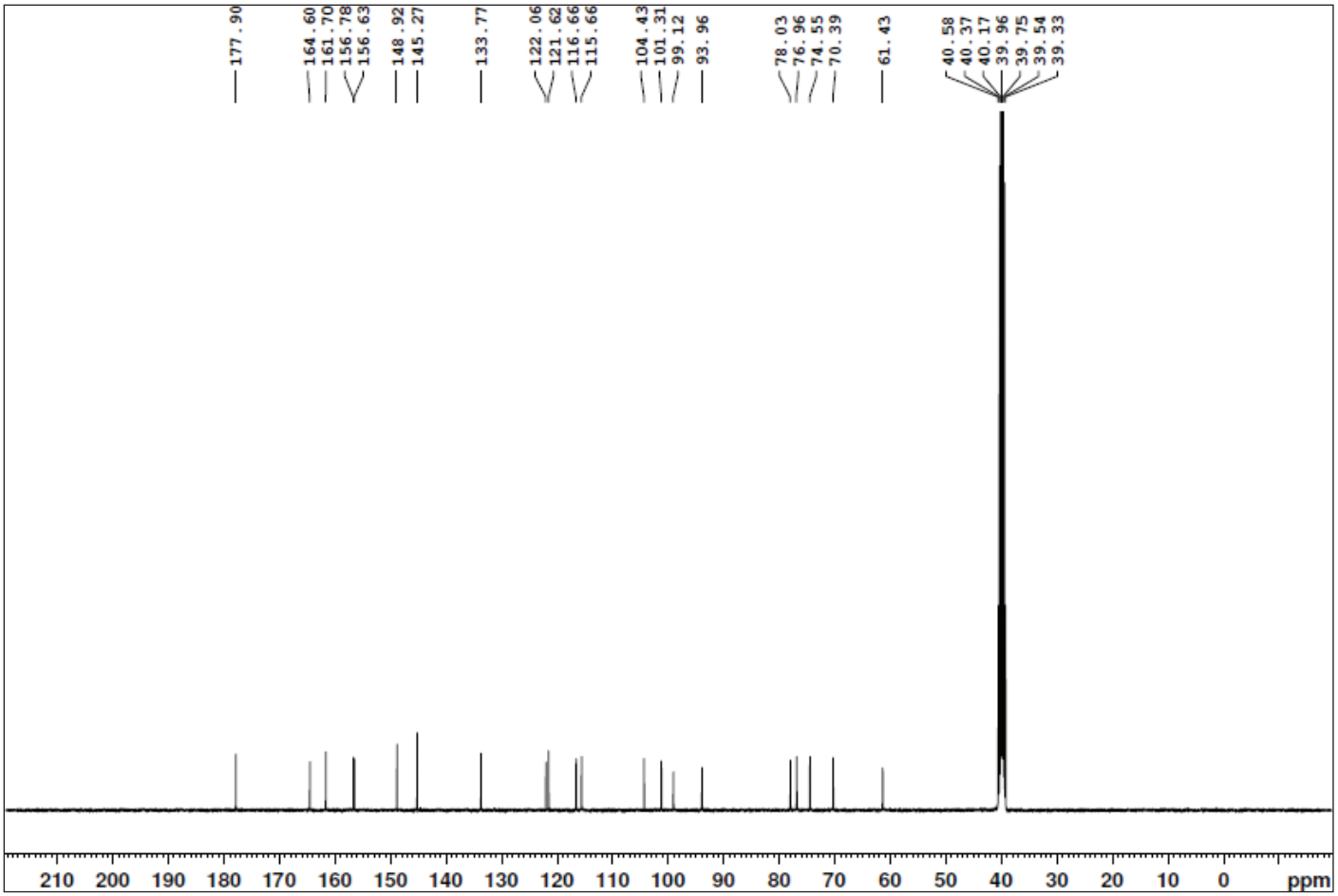

Figure 9S. [13]C-NMR spectra of isoquercitrin.

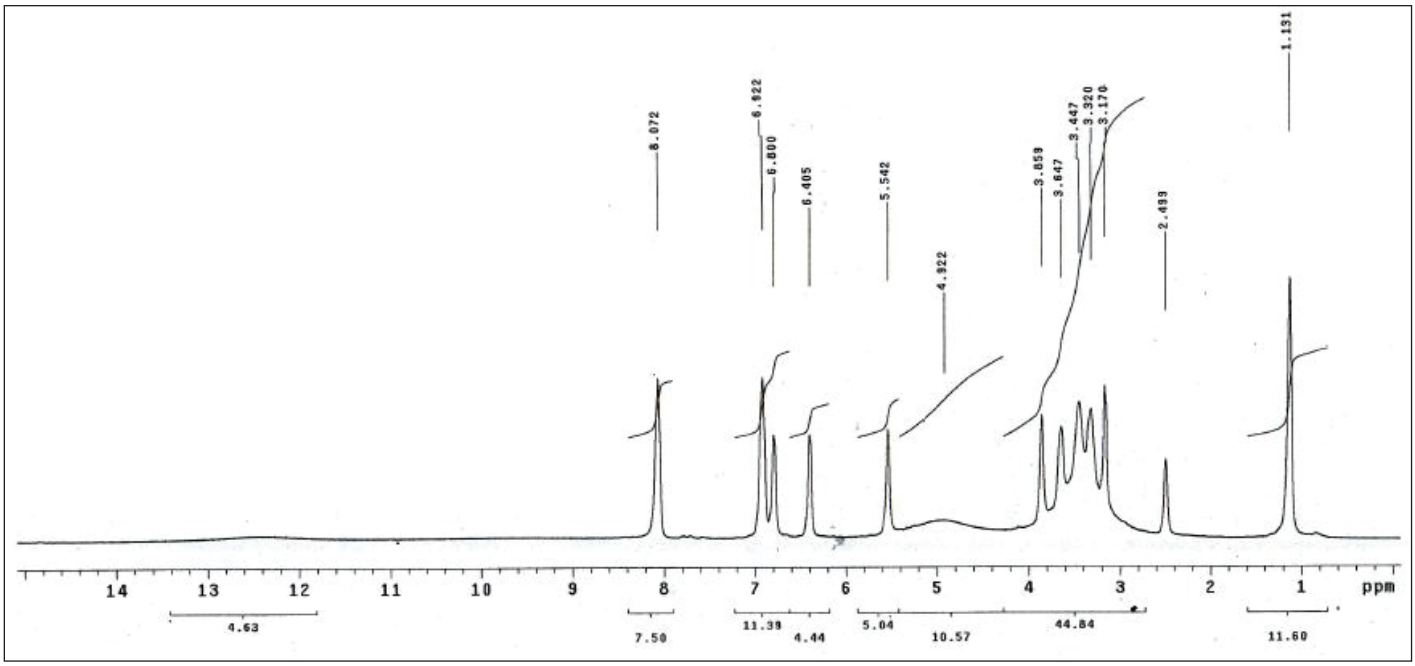

Figure 10S. [1]H-NMR spectra of kaempferin.

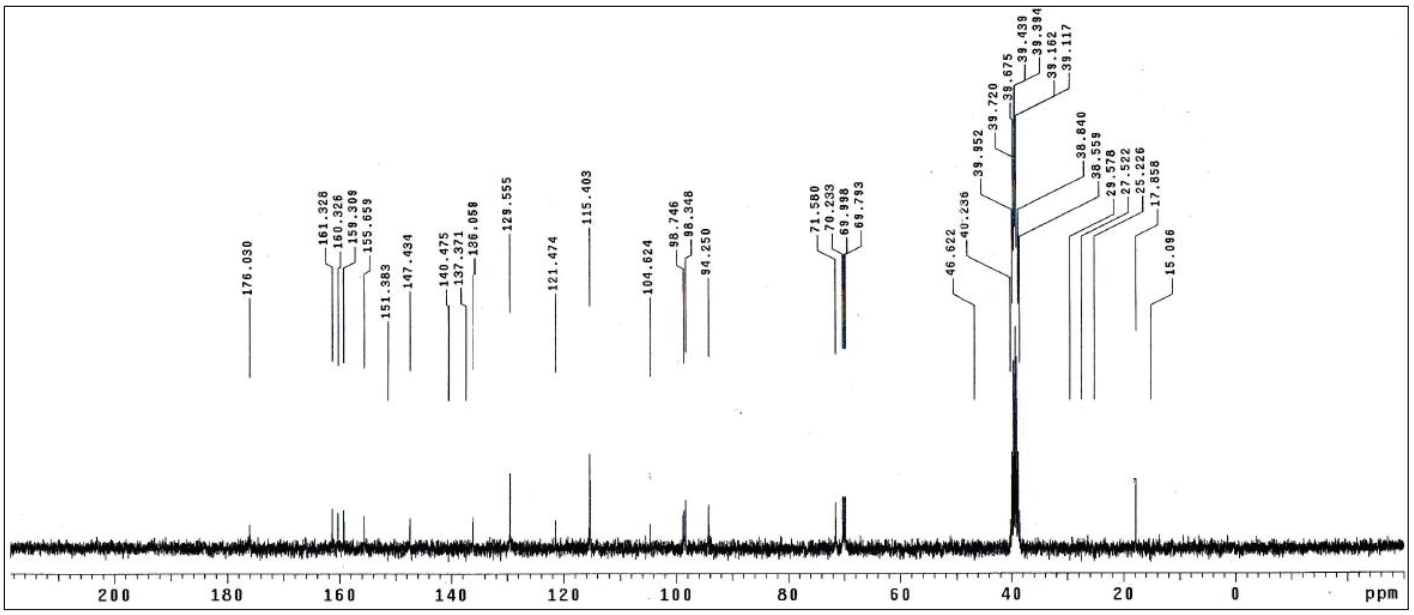

Figure 11S. ^{13}C-NMR spectra of kaempferin.

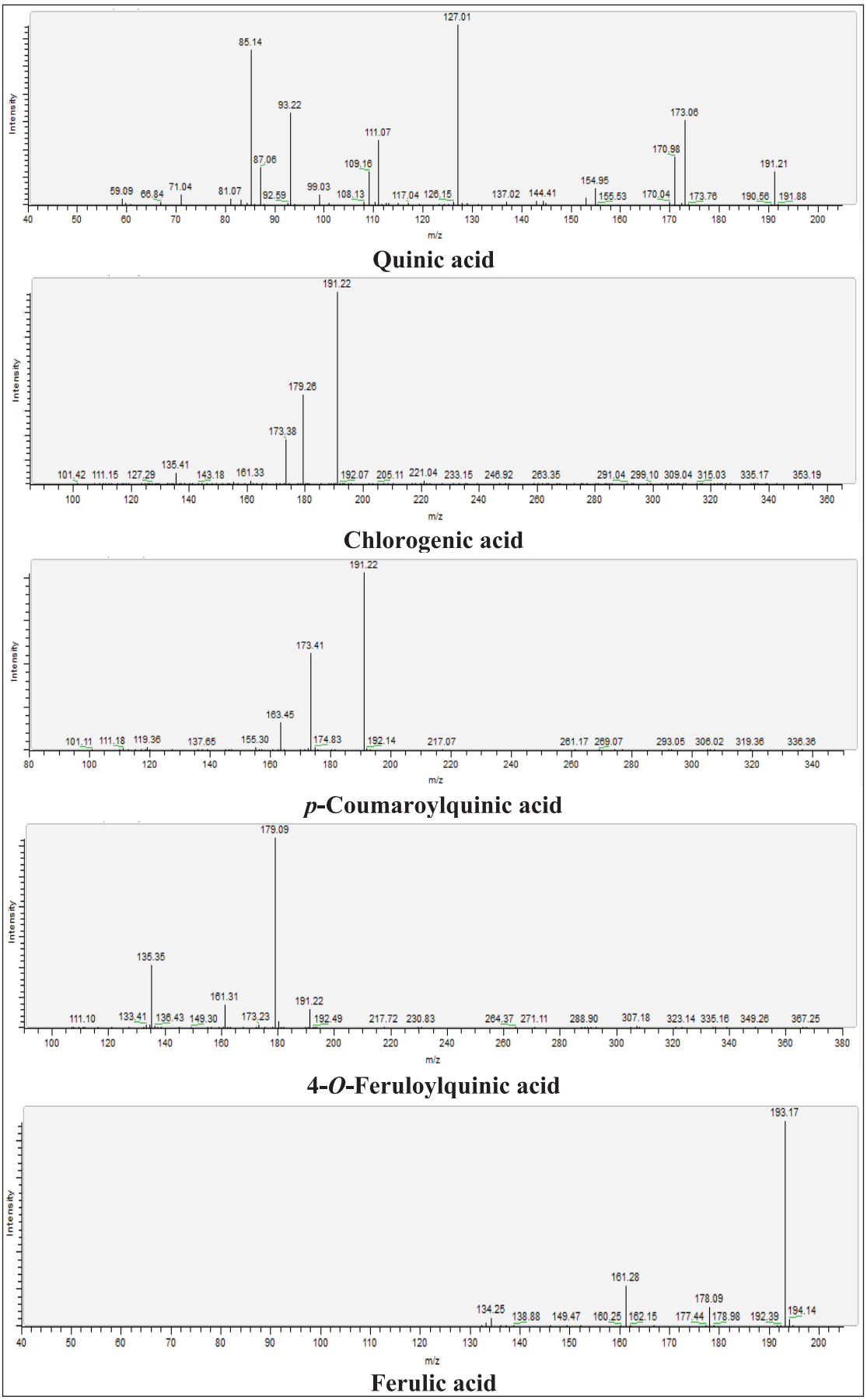

Figure 12S. MS/MS fragmentation pattern of Quinic acid, Chlorogenic acid, p-Coumaroylquinic acid, 4-O-Feruloylquinic acid, and Ferulic acid.

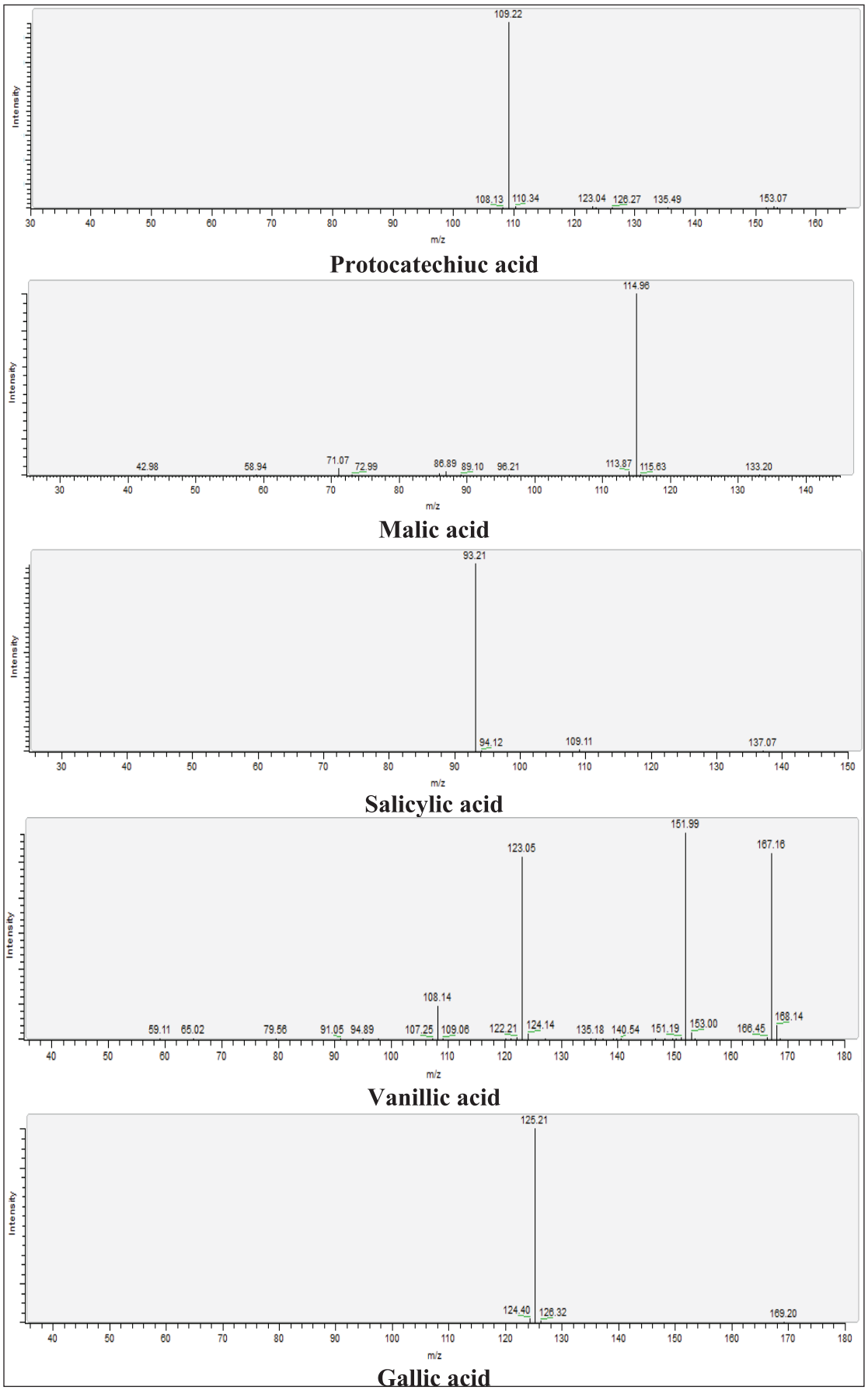

Figure 13S. MS/MS fragmentation pattern of Protocatechiuc acid, Malic acid, Salicylic acid, Vanillic acid, and Gallic acid.

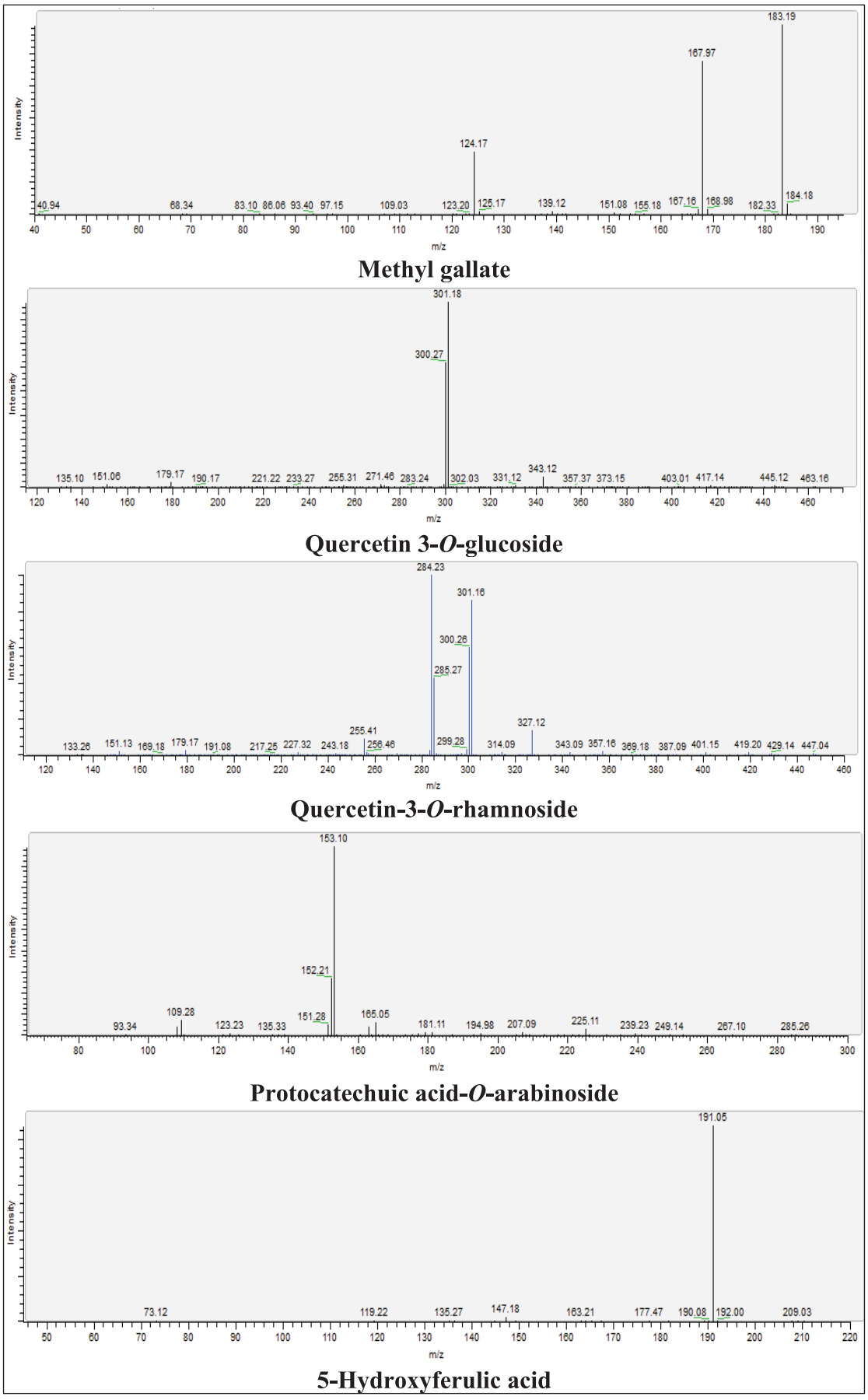

Figure 14S. MS/MS fragmentation pattern of Methyl gallate, Quercetin 3-O-glucoside, Quercetin 3-O-rhamnoside, Protocatechuic acid-O-arabinoside, and 5-Hydroxyferulic acid.

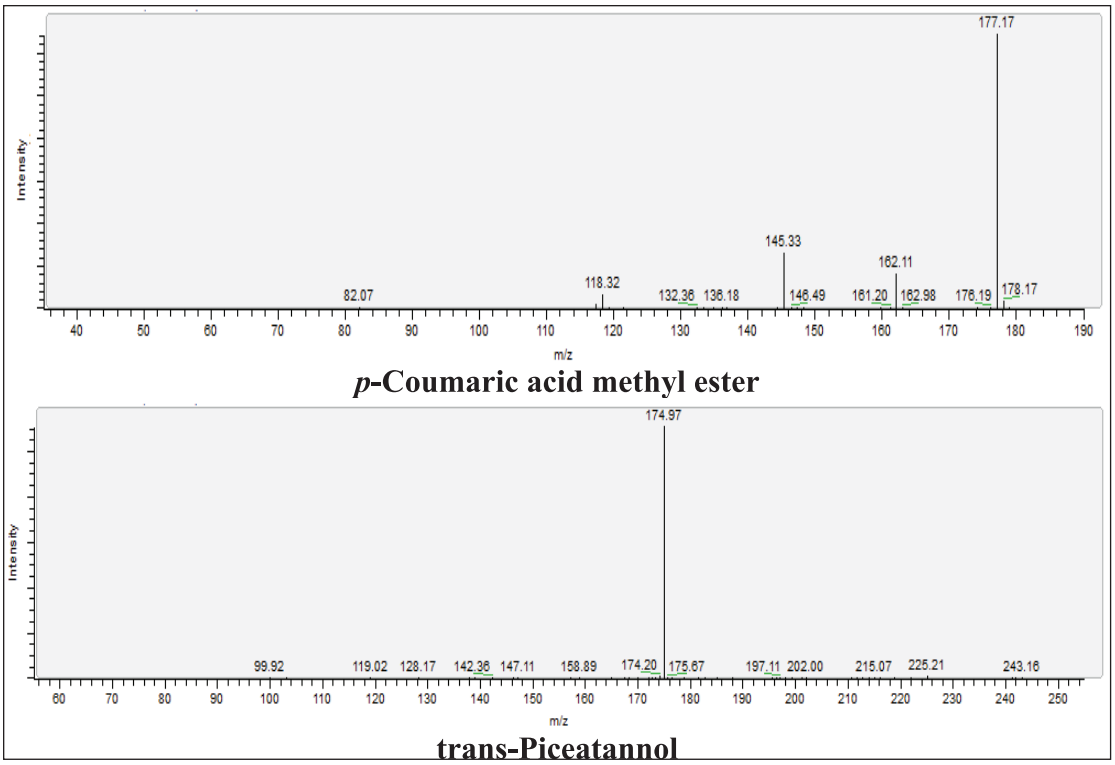

Figure 15S. MS/MS fragmentation pattern of p-Coumaric acid methyl ester, and trans-Piceatannol.

Table 1S. The docking results of extract components into the active site of Thioredoxin glutathione reductase (TGR).

Compound	Docking score (kcal/mol)	Interacting residues
Gallic acid (1)	−3.278	Arg322
Methyl gallate (2)	−4.718	Arg317, Ile319
Quercitrin (3)	−7.054	Asp433, Lys162, Thr442, Ser276
Isoquercitrin (4)	−11.370	Asp433, Arg393, Cys159, Gln158, Lys162, Ser276, Val157
Kaempferin (5)	−8.758	Asp433, Cys159, Thr442
Praziquantel	−6.407	Cys159, Thr442